

Quantum signatures of chaos, thermalization, and tunneling in the exactly solvable few-body kicked top

Shruti Dogra,^{*} Vaibhav Madhok,[†] and Arul Lakshminarayan[‡]
Department of Physics, Indian Institute of Technology Madras, Chennai 600036, India



(Received 29 August 2018; published 19 June 2019)

Exactly solvable models that exhibit quantum signatures of classical chaos are both rare as well as important—more so in view of the fact that the mechanisms for ergodic behavior and thermalization in isolated quantum systems and its connections to nonintegrability are under active investigation. In this work, we study quantum systems of few qubits collectively modeled as a kicked top, a textbook example of quantum chaos. In particular, we show that the three- and four-qubit cases are exactly solvable and yet, interestingly, can display signatures of ergodicity and thermalization. Deriving analytical expressions for entanglement entropy and concurrence, we see agreement in certain parameter regimes between long-time average values and ensemble averages of random states with permutation symmetry. Comparing with results using the data of a recent transmons-based experiment realizing the three-qubit case, we find agreement for short times, including a peculiar steplike behavior in correlations of some states. In the case of four qubits we point to a precursor of dynamical tunneling between what in the classical limit would be two stable islands. Numerical results for larger number of qubits show the emergence of the classical limit including signatures of a bifurcation.

DOI: [10.1103/PhysRevE.99.062217](https://doi.org/10.1103/PhysRevE.99.062217)

I. INTRODUCTION

In a modest pursuit of the esthetic attributed to the probabilist Feller that “the best consists of the general embodied in the concrete” [1], we consider extreme quantum cases of the kicked top, a widely studied textbook model of quantum chaos [2–13], which has also been implemented in experiments [14,15]. The general issues at hand are the emergence of classical chaos from a linear quantum substratum and, more recently, the role of quantum chaos in the thermodynamics of closed quantum systems [16–18]. Vigorous progress is being made in studying thermalization of isolated quantum systems that could be either time independent or periodically forced [15–32]. Entanglement within many-body states in such quantum chaotic systems drives subsystems to thermalization although the full state remains pure and of zero entropy, see Ref. [30] for a demonstration with cold atoms.

Quantum chaos [2,33] and, consequently, eigenstate thermalization hypothesis [18,21] enables one to use individual states for ensemble averages. For periodically driven systems that do not even conserve energy, a structureless “infinite-temperature” ensemble emerges in strongly nonintegrable regimes [26,28]. A recent three-qubit experiment, using superconducting Josephson junctions, that simulated the kicked top [15] (see also Ref. [34]) purported to remarkably demonstrate such a thermalization. Although such behavior has been attributed to nonintegrability [15,18], we exactly solve this three-qubit kicked top and also point out that it can be interpreted as a special case of an *integrable* model, the well-known transverse field Ising model. Interestingly, we

also solve the four-qubit case exactly, where there is no such evident connection to an already known integrable model.

The Arnold-Liouville notion of integrability requires sufficient number of independent constants of motion in involution. It is well known that in finite-dimensional quantum systems this notion can be debated, wherein any system is integrable as the projectors on eigenstates form a set of independent mutually commuting quantities, for example, see Ref. [35]. However, in this work, we use integrability more in the sense of the traditional definition of the existence of constants that arise from symmetries and whose forms are independent of the parameters of the system. This is a pragmatic approach and in line with current understanding that would classify the nearest-neighbor transverse field Ising model as integrable and one with an additional longitudinal field or a transverse field Ising model with nearest- as well as next-nearest-neighbor interactions as nonintegrable.

Nonintegrable, chaotic, systems may be solvable in some tangible sense; the textbook examples of the tent map and the bakers map are solvable, despite being completely chaotic. The Arnold cat map and its quantizations also admit analytical solutions despite being hyperbolic and chaotic. Nevertheless, this is very rare and restricted to abstract models. No known model that has a mixed phase space, with both regular and chaotic orbits, is also known to be exactly solvable in the same sense. Attempts at constructing such models include the piecewise linear “lazy bakers map.” The kicked top, in the limit of an infinite number of qubits, displays a standard transition to Hamiltonian chaos, including a mixed phase space, and it is remarkable that many of the features are already reflected in the solvable few-qubit cases as we show in this paper.

For example, we obtain explicit formulas for entanglements generated for the three- and four-qubit cases and the

^{*}shrutidogra.iiserm@gmail.com

[†]vmadhok@gmail.com

[‡]arul@iitm.ac.in

compare the former with data from the experiment in Ref. [15] and find very good agreement. The infinite-time average of single-qubit entanglement is found analytically for some initial states and at a special and large value of the forcing for all initially unentangled coherent states. These are shown to tend to that obtained from relevant (random matrix) ensembles, in some cases even exactly coinciding with them and thus displaying thermalization. These demonstrate that even in the deep quantum regime, the transition to what in the classical limit becomes chaos is reflected in the time-averaged entanglement. While the connections between chaos and entanglement in the semiclassical regime is now well studied [8–10,12,36–42], such systems are typically not analytically tractable and appeal is made to statistical modeling based on random matrix theory. Remarkably, there are interesting quantum effects in the few-body systems we study here. We find the presence of dynamical tunneling [43–47] between what appears in the classical limit as symmetric regular regions. This results in extremely slow convergence of subsystem entropies in the near-integrable regime that happens for some states of the four-qubit case. In the near-integrable regime the exactly calculable tunneling splitting is shown to result in this long-time dynamics. The kicked-top experiment involving the spin of cold Cs atoms has already observed such tunneling [14] but our observations provide a connection between the number of qubits and a system parameter at which such tunneling occurs. This may open windows to study the interplay of chaos and tunneling even in systems having a small number of qubits.

The model

The quantum kicked top is a combination of a rotation and a torsion; the Hamiltonian [2–4] is given by

$$H = \frac{\kappa_0}{2j} J_z^2 \sum_{n=-\infty}^{\infty} \delta(t - n\tau) + \frac{p}{\tau} J_y. \quad (1)$$

Here $J_{x,y,z}$ are components of the angular-momentum operator \mathbf{J} . The time between periodic kicks is τ . The Floquet map is the unitary operator,

$$\mathcal{U} = \exp[-i(\kappa_0/2j\hbar)J_z^2] \exp[-i(p/\hbar)J_y], \quad (2)$$

which evolves states just after a kick to just after the next. The parameter p measures rotation about the y axis, and in the following we set $\hbar = 1$ and $p = \pi/2$. The parameter κ_0 , which is the magnitude of a twist applied between kicks, controls the transition and measure of chaos. If it vanishes, then the dynamics is simply a rotation. As the magnitude of the total angular momentum is conserved, the quantum number j , with eigenvalues of \mathbf{J}^2 being $j(j+1)\hbar^2$, is a good one. The classical limit, when $j \rightarrow \infty$ is a map of the unit sphere phase space $X^2 + Y^2 + Z^2 = 1$ onto itself with the variables being $X, Y, Z = J_{x,y,z}/j$ and is given by (at i th iteration of the map)

$$\begin{aligned} X_i &= Z_{i-1} \cos(\kappa_0 X_{i-1}) + Y_{i-1} \sin(\kappa_0 X_{i-1}), \\ Y_i &= -Z_{i-1} \sin(\kappa_0 X_{i-1}) + Y_{i-1} \cos(\kappa_0 X_{i-1}), \\ Z_i &= -X_{i-1}. \end{aligned} \quad (3)$$

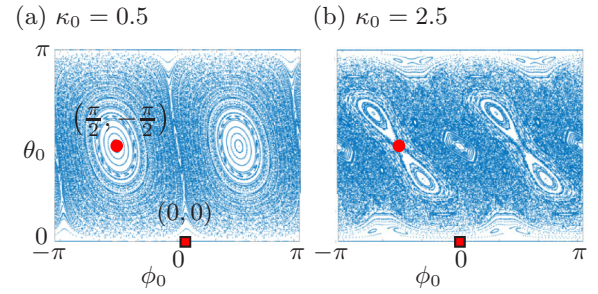


FIG. 1. (a) Regular and (b) mixed phase-space structures resulting from the classical chaotic dynamics. Points labeled with red square and red circle correspond to initial states $\Theta = 0, \Phi = 0$ on a period-4 orbit and $\Theta = \pi/2, \Phi = -\pi/2$ at the center of a regular island, respectively.

Numerical iterations for various different initial conditions, (X_0, Y_0, Z_0) , and for two strengths of the chaos, $\kappa_0 = 0.5$ and 2.5 , are shown in Fig. 1. These display what may be termed as regular and mixed phase-space structures, respectively, with the measure of chaotic orbits at κ_0 being negligibly small. For $\kappa_0 = 0$ the classical map is evidently integrable, being just a rotation, but for $\kappa_0 > 0$ chaotic orbits appear in the phase space and when $\kappa_0 > 6$ it is essentially fully chaotic. Connection to a many-body model can be made by considering the large \mathbf{J} spin as the total spin of spin = $1/2$ qubits, replacing $J_{x,y,z}$ with $\sum_{l=1}^{2j} \sigma_l^{x,y,z}/2$ [8,48]. The Floquet operator is then that of $2j$ qubits, an Ising model with all-to-all homogeneous coupling and a transverse magnetic field:

$$\mathcal{U} = \exp\left(-i\frac{\kappa_0}{4j} \sum_{l < l'=1}^{2j} \sigma_l^z \sigma_{l'}^z\right) \exp\left(-i\frac{\pi}{4} \sum_{l=1}^{2j} \sigma_l^y\right). \quad (4)$$

Here $\sigma_l^{x,y,z}$ are the standard Pauli matrices, and an overall phase is neglected. In general only the $2j+1$ -dimensional permutation symmetric subspace of the full 2^{2j} -dimensional space is relevant to the kicked top.

Note that for κ_0 that are multiples of $2\pi j$, \mathcal{U} is a local operator and does not create entanglement, and we therefore restrict attention to the interval $\kappa_0 \in [0, \pi j]$. The case of two qubits, $j = 1$, has been analyzed in Ref. [49], wherein interesting arguments have been proposed for the observation of structures not linked to the classical limit. In this case, several quantum correlation measures were also calculated in Ref. [50]. Entanglement dependence on bifurcations and scars for higher j values was explored in a related work in Ref. [51]. For $j = 3/2$, the three-qubit case, as all-to-all is just nearest neighbor with periodic boundary conditions, it is a nearest-neighbor kicked transverse Ising model, known to be integrable [52,53]. The Jordan-Wigner transformation renders it a model of noninteracting fermions that can be immediately solved. This is also the case that was considered in the superconducting Josephson junction experiment [15] that treated it as chaotic. For higher values of the spin j , the model maybe considered few-body realizations of nonintegrable systems.

In the following we will mostly be studying time evolution from initial states that are localized in the spherical phase space, and these are the standard $SU(2)$ coherent states. Permutation symmetric initial states used are coherent states

located at

$$\begin{aligned} X_0 &= \sin \theta_0 \cos \phi_0, \\ Y_0 &= \sin \theta_0 \sin \phi_0, \\ Z_0 &= \cos \theta_0, \end{aligned} \quad (5)$$

on the phase-space sphere and given by [54,55],

$$|\theta_0, \phi_0\rangle = \otimes^{2j} [\cos(\theta_0/2)|0\rangle + e^{-i\phi_0} \sin(\theta_0/2)|1\rangle]. \quad (6)$$

II. ANALYTICAL SOLUTION OF THE THREE-QUBIT CASE

From Eq. (4), the unitary Floquet operator for $2j = 3$ qubits that simulate the dynamics of a spin-3/2 under a kicked top Hamiltonian is given by

$$\begin{aligned} \mathcal{U} &= \exp \left[-i \frac{\kappa_0}{6} (\sigma_1^z \sigma_2^z + \sigma_2^z \sigma_3^z + \sigma_3^z \sigma_1^z) \right] \\ &\quad \exp \left[-i \frac{\pi}{4} (\sigma_1^y + \sigma_2^y + \sigma_3^y) \right], \end{aligned} \quad (7)$$

where all the terms have their usual meanings as defined in Sec. IA. The solution to the three-qubit case proceeds from the general observation that

$$[\mathcal{U}, \otimes_{i=1}^3 \sigma_i^y] = 0,$$

i.e., there is an ‘‘up-down’’ or parity symmetry.

The standard four-dimensional spin quartet permutation symmetric space with $j = 3/2$, $\{|000\rangle, |W\rangle = (|001\rangle + |010\rangle + |100\rangle)/\sqrt{3}, |\bar{W}\rangle = (|110\rangle + |101\rangle + |011\rangle)/\sqrt{3}, |111\rangle\}$ is parity symmetry adapted to form the basis

$$|\phi_1^\pm\rangle = \frac{1}{\sqrt{2}}(|000\rangle \mp i|111\rangle), \quad (8)$$

$$|\phi_2^\pm\rangle = \frac{1}{\sqrt{2}}(|W\rangle \pm i|\bar{W}\rangle). \quad (9)$$

These are parity eigenstates such that $\otimes_{i=1}^3 \sigma_i^y |\phi_j^\pm\rangle = \pm |\phi_j^\pm\rangle$. Notations employed reflect the usage of $|W\rangle$ as the standard W state of quantum information and the $|\phi_1^\pm\rangle$ correspond to the standard GHZ (Greenberger-Horne-Zeilinger) quantum states. To visualize these basis states the contour plots of their quasiprobability distribution in the phase space is shown in Fig. 2. We see that while the GHZ class of states are localized prominently at the poles of the sphere, the superposition of the W states are localized at the equatorial plane and peak at $(\theta_0 = \pi/2, \phi_0 = \pm\pi/2)$. Interestingly, these points correspond to low-order periodic points for the classical map and form the most important initial states to evolve for the quantum system. In this basis, the unitary operator \mathcal{U} is given by

$$\mathcal{U} = \begin{pmatrix} \mathcal{U}_+ & 0 \\ 0 & \mathcal{U}_- \end{pmatrix}, \quad (10)$$

where 0 is a 2×2 null matrix, and 2×2 -dimensional blocks \mathcal{U}_+ (\mathcal{U}_-) are written the bases $\{\phi_1^+, \phi_2^+\}$ ($\{\phi_1^-, \phi_2^-\}$), in the positive- (negative-) parity subspaces, respectively. Explicitly, these have matrix elements

$$\mathcal{U}_\pm = \pm e^{\mp \frac{i\pi}{4}} e^{-i\kappa} \begin{pmatrix} \frac{i}{2} e^{-2i\kappa} & \mp \frac{\sqrt{3}}{2} e^{-2i\kappa} \\ \pm \frac{\sqrt{3}}{2} e^{2i\kappa} & -\frac{i}{2} e^{2i\kappa} \end{pmatrix}. \quad (11)$$

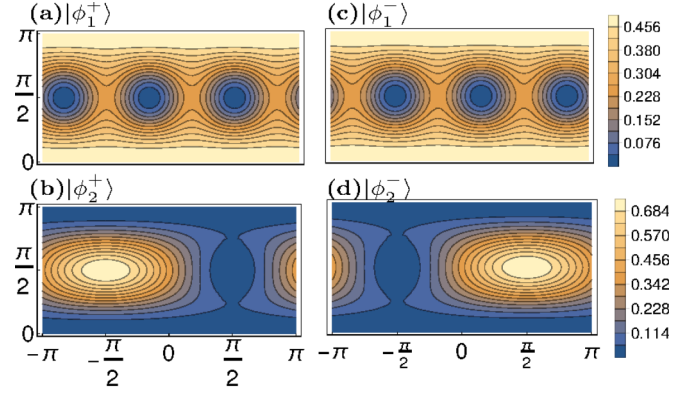


FIG. 2. Husimi (quasiprobability distribution, $|\langle \phi_i | \theta_0, \phi_0 \rangle|^2$) plots for a set of 4 three-qubit bases states ($|\phi_i\rangle$), where $|\theta_0, \phi_0\rangle$ is an arbitrary three-qubit, parametrized by (θ_0, ϕ_0) .

For simplicity the parameter $\kappa = \kappa_0/6$ is used in these expressions. Expressing \mathcal{U}_+ as a rotation $e^{-i\gamma\hat{\sigma}\cdot\hat{\eta}}$ by angle γ about an axis $\hat{\eta} = \sin \theta \cos \phi \hat{x} + \sin \theta \sin \phi \hat{y} + \cos \theta \hat{z}$, up to a phase. On comparison with Eq. (11), we obtain $\cos \gamma = \frac{1}{2} \sin 2\kappa$, $\phi = \pi/2 + 2\kappa$, and $\sin \theta \sin \gamma = \sqrt{3}/2$. To evolve initial states we need \mathcal{U}^n and therefore \mathcal{U}_\pm^n , which is explicitly given by

$$\mathcal{U}_\pm^n = (\pm 1)^n e^{-in(\pm\frac{\pi}{4} + \kappa)} \begin{pmatrix} \alpha_n & \mp \beta_n^* \\ \pm \beta_n & \alpha_n^* \end{pmatrix}, \quad (12)$$

where

$$\alpha_n = T_n(\chi) + \frac{i}{2} U_{n-1}(\chi) \cos 2\kappa \quad \text{and} \quad (13)$$

$$\beta_n = (\sqrt{3}/2) U_{n-1}(\chi) e^{2i\kappa}. \quad (14)$$

The Chebyshev polynomials $T_n(\chi)$ and $U_{n-1}(\chi)$ are defined as $T_n(\chi) = \cos(n\gamma)$ and $U_{n-1}(\chi) = \sin(n\gamma)/\sin \gamma$ [56] with $\chi = \cos \gamma = \sin(2\kappa)/2$. Also note that $|\alpha_n|^2 + |\beta_n|^2 = 1$. This follows both from the unitarity of \mathcal{U}_\pm as well as a polynomial Pell identity satisfied by the Chebyshev polynomials, namely

$$T_n^2(x) + (1 - x^2)U_{n-1}^2(x) = 1. \quad (15)$$

Remarkably, one can also view this as a new proof of the Pell identity satisfied by Chebyshev polynomials through the unitarity of quantum mechanics.

Note also that the range of χ is restricted in this case to $|\chi| \leq 1/2$, which in addition to the general identity $|T_n(\chi)| \leq 1$ also implies that $|U_{n-1}(\chi)| \leq 2/\sqrt{3}$, which follows from Eq. (14).

It is now straightforward to do time evolution for an arbitrary three-qubit permutation symmetric state and thereafter study its various properties. We further analyze two widely different three-qubit states [(i) $|0, 0\rangle$ and (ii) $|\pi/2, -\pi/2\rangle$] in detail. For these two states, we obtain the exact expressions for linear entropy of a single-party reduced-density matrix, time average of the linear entropy, and concurrence between any two qubits as a measure of entanglement. These analytical expressions are verified numerically and also compared, where possible, with the data from the superconducting transmon qubits experiment in Ref. [15]. We particularly considered

these two examples due to their preferential behaviors as classical phase-space structures. A three-qubit state $\otimes^3|0\rangle$ corresponds to coherent state at $|0, 0\rangle$ which is on the period-4 orbit whose classical correspondence is shown with a square in Fig. 1, while $\otimes^3|+\rangle_y$ corresponds to the coherent state at $|\pi/2, -\pi/2\rangle$, which is a fixed point on the classical phase space. This becomes unstable as we move from regular to mixed phase space at $\kappa_0 = 2$ and is indicated by a circle in Fig. 1.

A. Initial state $|000\rangle = |\theta_0 = 0, \phi_0 = 0\rangle$

Let us consider the state on the period-4 orbit, corresponding to the coherent state at $|0, 0\rangle$ which is $\otimes^3|0\rangle$.

$$\begin{aligned} |\psi_n\rangle &= \mathcal{U}^n|000\rangle = \frac{1}{\sqrt{2}}\mathcal{U}^n(|\phi_1^+\rangle + |\phi_1^-\rangle) \\ &= \frac{1}{\sqrt{2}}(\mathcal{U}_+^n|\phi_1^+\rangle + \mathcal{U}_-^n|\phi_1^-\rangle) \\ &= \frac{1}{2}e^{-in(\frac{3\pi}{4} + \kappa)}\{(1 + i^n)(\alpha_n|000\rangle + i\beta_n|\overline{W}\rangle) \\ &\quad + (1 - i^n)(i\alpha_n|111\rangle - \beta_n|W\rangle)\}. \end{aligned} \quad (16)$$

From this the one- and two-qubit reduced-density matrices $\rho_1(n) = \text{tr}_{2,3}(|\psi_n\rangle\langle\psi_n|)$, $\rho_{12}(n) = \text{tr}_3(|\psi_n\rangle\langle\psi_n|)$ are obtained. The entanglement of one qubit with the other two is found as the linear entropy $1 - \text{Tr}[\rho_1(n)^2]$, and from the two-qubit reduced matrix, the entanglement between two qubits is found as the concurrence [57].

1. The linear entropy

It turns out that for even values of the time n , say, $n = 2m$, $\rho_1(2m)$ is diagonal, whose diagonal elements are $\lambda(2m, \kappa_0)$ and $1 - \lambda(2m, \kappa_0)$, from which the linear entropy,

$$S_{(0,0)}^{(3)}(2m, \kappa_0) = 2\lambda(2m, \kappa_0)[1 - \lambda(2m, \kappa_0)], \quad (17)$$

where the eigenvalue

$$\lambda(2m, \kappa_0) = \frac{1}{2}U_{2m-1}^2(\chi) = \frac{2}{3}|\beta_{2m}|^2. \quad (18)$$

For odd values of n , $\rho_1(n)$ is not diagonal, but a peculiar result is obtained. One can evolve the even $n = 2m$ states one step backward in time,

$$|\phi_{2m-1}\rangle = \mathcal{U}^{-1}|\phi_{2m}\rangle, \quad (19)$$

where \mathcal{U} is the Floquet operator in Eq. (7). Let m itself be an even integer, which implies that only the first half of the state in Eq. (16) survives. Then, to an overall phase, using the nonlocal part of the unitary operator \mathcal{U} , the state to local unitary operations is

$$\begin{aligned} |\phi_{2m-1}\rangle_{\text{loc}} &= e^{i\kappa(\sigma_1^z\sigma_2^z + \sigma_2^z\sigma_3^z + \sigma_3^z\sigma_1^z)}(\alpha_{2m}|000\rangle + i\beta_{2m}|\overline{W}\rangle), \\ &= e^{3i\kappa}\alpha_{2m}|000\rangle + ie^{-i\kappa}\beta_{2m}|\overline{W}\rangle, \\ &= \mathcal{V} \otimes \mathcal{V} \otimes \mathcal{V}|\phi_{2m}\rangle, \end{aligned} \quad (20)$$

where single-qubit unitary operator $\mathcal{V} = e^{i\kappa\sigma_z}$. Thus the three-qubit state $|\psi_{2m-1}\rangle$, after odd-numbered implementations of the unitary operator \mathcal{U} are local unitarily equivalent to the state obtained after $2m$ implementations of \mathcal{U} and hence all entanglement properties including entropy and concurrence

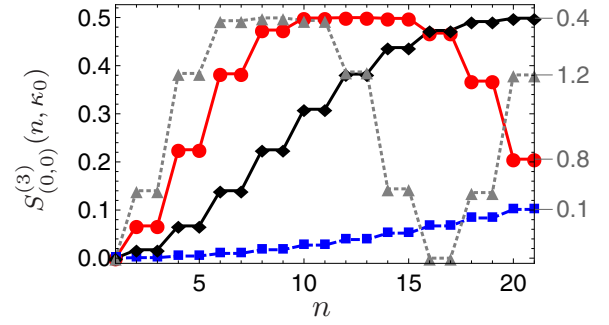


FIG. 3. Linear entropy of a single-qubit reduced state versus n is plotted for initial state $|000\rangle$ at different values of $\kappa_0 = 0.1, 0.4, 0.8$, and 1.2 as labeled on the right end of each curve.

are left unchanged for an odd-to-even time step. A similar situation holds when m is odd. Therefore, for a pair of consecutive implementations, entanglement among the qubits does not change, giving rise to steplike features in the variation of entropy and concurrence with time. In particular,

$$S_{(0,0)}^{(3)}(2n-1, \kappa_0) = S_{(0,0)}^{(3)}(2n, \kappa_0), \quad n = 1, 2, \dots \quad (21)$$

This steplike feature in the variation of entropy is illustrated for a few values of κ_0 in Fig. 3. It is seen that there is a monotonic increase of the initial rate of entropy production as a function of κ_0 . This gives way to nonmonotonic behavior both in time and in the parameter κ_0 . The initial rate can be simply quantified by the entanglement entropy at $n = 1$. Again using the linear entropy we have as a special case that

$$S_{(0,0)}^{(3)}(1, \kappa_0) = \sin^2(\kappa_0/3)[1 - \frac{1}{2}\sin^2(\kappa_0/3)], \quad (22)$$

which increases monotonically until $\kappa_0 = 3\pi/2$ where the maximum value of $1/2$ is acquired, which is also the upper bound. We will see that the case of $\kappa_0 = 3\pi/2$ is one of maximal chaos in some sense for $j = 3/2$.

For small κ_0 , the growth of the entropy is $S_{(0,0)}^{(3)}(1, \kappa_0) \approx \kappa_0^2/9$. From Fig. 3 it is seen that even for small values of κ_0 the entropy eventually becomes large and the maximum allowed value of $1/2$ is reached. As the classical dynamics for small κ_0 is regular, the large value of the entanglement reached is intriguing. We now estimate the time it takes for the entanglement to reach nearly the maximum value. The state in Eq. (16) clearly distinguishes times modulo 4. If the time n is odd and β_n vanishes (the conditions under which this happens is discussed below), then the resultant state is the GHZ one with an equal superposition of $|000\rangle$ and $|111\rangle$ which is such that the reduced-density matrices are maximally mixed and hence have maximum entropy. If the time n is even and β_n vanishes, then there is no entanglement as the state becomes a tensor product, as is also apparent from Eqs. (17) and (18).

From Eq. (14), the vanishing of β_n corresponds to the zeros of the Chebyshev polynomials of the second kind, $U_{n-1}(\chi)$, which are at $\chi = \chi_k = \cos(\pi k/n)$ and $k = 1, 2, \dots, n-1$. Thus we are looking for values of n such that

$$\frac{1}{2}\sin(\kappa_0/3) = \cos(\pi k/n), \quad (23)$$

which may be found from the continued fraction convergents of $r = \cos^{-1}[\sin(\kappa_0/3)/2]/\pi$. For small $\kappa_0 (\ll 1)$, $r \lesssim 1/2$ the first nonzero convergent is $1/2$ and therefore the second is of

the form $a_1/(2a_1 + 1)$ where a_1 is an integer. Identifying this with k/n we see that n is an odd integer and hence this corresponds to the case of maximum, or at least near-maximum, entanglement. Taylor expanding the \sin and the \cos^{-1} and retaining the lowest-order terms then gives an estimate of the time n_* at which the entanglement, for the first time, reaches nearly the maximum as

$$n_* \approx 2 \left[\frac{3\pi}{2\kappa_0} - \frac{1}{2} \right] + 1 \approx \left[\frac{3\pi}{\kappa_0} \right], \quad (24)$$

and the time at which it gets unentangled, for the first time, is $\sim 2n_*$. We see from Fig. 3 that these are excellent estimates even when κ_0 is as large as 0.4 or 0.8.

The formation of nonclassical states such as the GHZ in this instance is a forerunner of dynamical tunneling as for small κ_0 the islands at the ‘‘poles’’ of the phase-space sphere can start to localize states for large values of j . This effect is seen prominently in the long-time averages. The intriguing increase of entanglement with time, even for small κ_0 , in these states therefore has very different origins than the nonintegrability of the kicked top.

2. Long-time-averaged linear entropy

The infinite-time average of the linear entropy, which can be easily obtained from Eq. (17), maybe inaccessible experimentally but is of definite interest from the point of view of thermalization and it also is a way to study the influence of the parameter κ_0 directly. We need to use only even values of the time as for this state due to the property discussed above. We have

$$S_{(0,0)}^{(3)}(2m, \kappa_0) = U_{2m-1}^2(\chi) - \frac{1}{2} U_{2m-1}^4(\chi), \quad (25)$$

$$= \frac{\sin^2 2m\gamma}{\sin^2 \gamma} - \frac{1}{2} \frac{\sin^4 2m\gamma}{\sin^4 \gamma}. \quad (26)$$

The time-averaged linear entropy is thus given by

$$\langle S_{(0,0)}^{(3)}(\kappa_0) \rangle = \lim_{N \rightarrow \infty} \frac{1}{N} \sum_{m=0}^{N-1} S_{(0,0)}^{(3)}(2m, \kappa), \quad (27)$$

$$= \frac{1}{2 \sin^2 \gamma} - \frac{3}{16 \sin^4 \gamma}, \quad (28)$$

where we have used that $\langle \sin^2(2m\gamma) \rangle = 1/2$ and $\langle \sin^4(2m\gamma) \rangle = 3/8$, assuming that $\gamma \neq 0, \pi/2, \pi$. Further, using $\cos \gamma = \frac{1}{2} \sin 2\kappa = \frac{1}{2} \sin(\kappa_0/3)$, we obtain the average explicitly in terms of κ_0 as

$$\langle S_{(0,0)}^{(3)}(\kappa_0) \rangle = \frac{5 - 2 \sin^2(\kappa_0/3)}{[4 - \sin^2(\kappa_0/3)]^2}, \quad 0 < \kappa_0 < 3\pi. \quad (29)$$

This attains its maximum value of $1/3$ at $\kappa_0 = 3\pi/2$. This may be used as a probe to understand the process of thermalization, which is discussed later in this section. However, it is appropriate to point out that $\langle S_{(0,0)}^{(3)}(\kappa_0) \rangle$ is discontinuous at $\kappa_0 = 0$ as it vanishes at $\kappa_0 = 0$ but is $5/16$ for arbitrarily small and nonzero values. Thus in this deep quantum regime, the state that starts off from the period-4 orbit gets entangled to a large extent even when the orbit is classically stable. However, this is reflected in the infinite-time average which includes highly nonclassical timescales, as discussed above.

3. Concurrence

While the linear entropy is a measure of entanglement of one-qubit with the other two, the entanglement between any two qubits is quantified by the concurrence. Due to the permutation symmetry in the state it does not matter which two qubits are considered; there is only one concurrence. The concurrence is derived from the two-qubit reduced-density matrix, as opposed to the entanglement of one qubit which needs only the one-qubit state. If ρ_{12} is the two-qubit state, then its concurrence is given by

$$\mathcal{C}(\rho_{12}) = \max(0, \sqrt{\lambda_1} - \sqrt{\lambda_2} - \sqrt{\lambda_3} - \sqrt{\lambda_4}), \quad (30)$$

where λ_i are eigenvalues in decreasing order of $(\sigma_y \otimes \sigma_y) \rho_{12} (\sigma_y \otimes \sigma_y) \rho_{12}^*$, where ρ_{12}^* is conjugation in the standard (σ_z) basis.

An exact expression for concurrence among any two qubits in the state $|\psi_n\rangle$ of Eq. (16) is possible to obtain explicitly as the two-qubit state is an ‘‘X state’’ [58] when the time n is even. A two-qubit reduced-density operator of $\rho_{12}(n)$ obtained by tracing out one of the qubits in $|\psi_n\rangle\langle\psi_n|$ is given by

$$\rho_{12}(n) = \begin{pmatrix} |\alpha_n|^2 & 0 & 0 & -\frac{i}{\sqrt{3}} \alpha_n \beta_n^* \\ 0 & \frac{1}{3} |\beta_n|^2 & \frac{1}{3} |\beta_n|^2 & 0 \\ 0 & \frac{1}{3} |\beta_n|^2 & \frac{1}{3} |\beta_n|^2 & 0 \\ \frac{i}{\sqrt{3}} \alpha_n^* \beta_n & 0 & 0 & \frac{1}{3} |\beta_n|^2 \end{pmatrix}, \quad (31)$$

whose concurrence is found from the general formula for the X states [58],

$$\begin{aligned} \mathcal{C}(n, \kappa_0) &= 2 \max \left[0, \frac{1}{3} |\beta_n|^2 - \frac{1}{\sqrt{3}} |\alpha_n| |\beta_n|, \right. \\ &\quad \left. - \left(\frac{1}{3} |\beta_n|^2 - \frac{1}{\sqrt{3}} |\alpha_n| |\beta_n| \right) \right] \\ &= 2 \left| \frac{1}{3} |\beta_n|^2 - \frac{1}{\sqrt{3}} |\alpha_n| |\beta_n| \right| \\ &= |U_{n-1}(\chi)| \left| \frac{1}{2} |U_{n-1}(\chi)| - \sqrt{1 - \frac{3}{4} |U_{n-1}(\chi)|^2} \right|, \end{aligned} \quad (32)$$

where we recall for convenience that $\chi = \cos \gamma = \sin(2\kappa)/2 = \sin(\kappa_0/3)/2$. This is valid when the time n is even, but from the arguments presented in the discussion of the entanglement entropy it follows that

$$\mathcal{C}(2m - 1, \kappa_0) = \mathcal{C}(2m, \kappa_0), \quad m = 1, 2, \dots \quad (33)$$

See Fig. 4 for the variation of the concurrence with time for the same values of κ_0 as used in the previous figure. As with the case of the linear entropy, the concurrence initially increases monotonically with κ_0 as well as with time. Once again it is of interest to see how much concurrence is produced in simply the first step and this is

$$\mathcal{C}(1, \kappa_0) = \sin(\kappa_0/3) \left[\sqrt{1 - \frac{3}{4} \sin^2(\kappa_0/3)} - \frac{1}{2} \sin(\kappa_0/3) \right], \quad (34)$$

which is valid when $0 \leq \kappa_0 \leq 3\pi$, and beyond this the concurrence is periodic. Interestingly, this is monotonic in κ_0

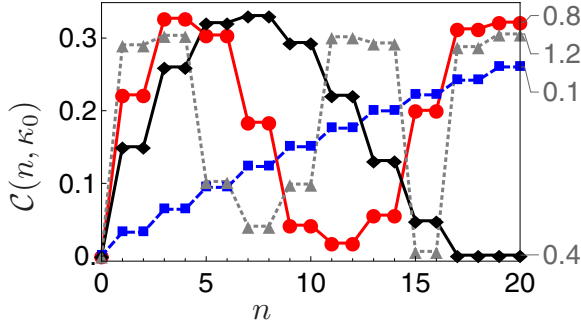


FIG. 4. Concurrence of a two-qubit reduced state versus n is plotted for $\kappa_0 = 0.1, 0.4, 0.8,$ and 1.2 as labeled on the right end of each curve.

only until $\kappa_0 = \pi/2$, where it attains the maximum value of $(\sqrt{13} - 1)/8 \approx 0.3257$. This is in contrast to the linear entropy or entanglement of one qubit with the rest which grows until $\kappa_0 = \pi$.

It is useful to compare the concurrence and entanglement entropy directly and this is illustrated in Fig. 5 where for four values of κ_0 these are plotted as a function of time. It is seen that while initially both of them grow, after a certain time, the concurrence starts to decrease while the entanglement continues to increase. This is the phase where entanglement is started to be shared globally rather than in bipartite manner. In this case of only three qubits, this implies that tripartite entanglement starts to significantly grow after this time. It is also seen that when the entanglement entropy is the maximum possible, concurrence is at a minimum and sometimes vanishes. This is consistent with the fact that entanglement is monogamous and hence cannot be simultaneously shared among the three qubits. It is interesting that the simple formulas derived for this system illustrates these more general

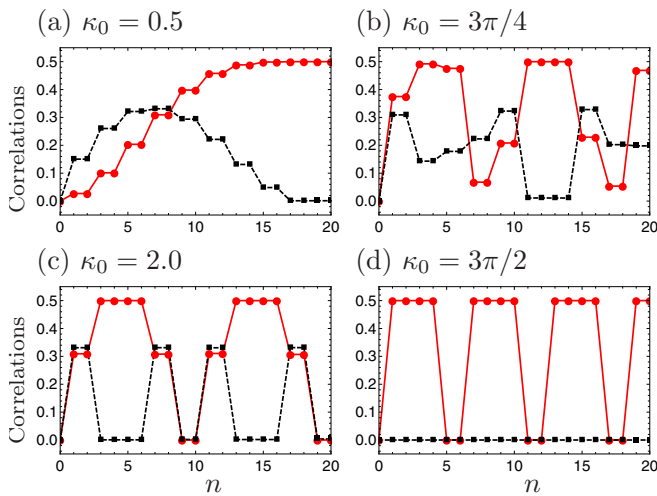


FIG. 5. Solid curve with circles and dashed curve with squares show the variation of entropy of a single-qubit reduced state and concurrence between a pair of two qubits, respectively, with n as three-qubit initial state $|000\rangle$ evolves under \mathcal{U}^n . Parts (a), (b), (c), and (d) correspond to different values of chaoticity parameter (κ_0) as mentioned.

features. In particular it is clear from Eqs. (17) and (32) that while both the entanglement and concurrence vanish when $U_{n-1}(\chi) = 0$, the concurrence also vanishes when $U_{n-1}(\chi) = \pm 1$, a case that corresponds to a maximum entanglement. More discussion on this is also found in Ref. [34].

A curious case is obtained when $\kappa_0 = 3\pi/2$ when $\cos \gamma = 1/2$ and hence $\gamma = \pi/3$ and $U_{n-1}(\chi) = \sin(2\pi n/3)/\sin(\pi/3)$, which takes the value 0 when $n \pmod{3} = 0$, is +1 when $n \pmod{3} = 1$ and is -1 when $n \pmod{3} = 2$. This implies that when $n \pmod{6} \neq 0$ or -1 the entanglement entropy is the maximum possible value of $1/2$ while the concurrence vanishes for all values of time n , as seen in the last panel of Fig. 5. Thus in this case the entanglement is shared only in a tripartite manner. We will return to this case later, but note here that indeed special values of such parameters in Floquet spin systems display similar behavior with large multipartite entanglement [59].

B. Initial state $|++\rangle_y = |\theta_0 = \pi/2, \phi_0 = -\pi/2\rangle$ and beyond

We considered in some detail the fate of the state $|000\rangle$, and we now study the case of the three-qubit state $|\psi_0\rangle = |++\rangle_y$, where $|+\rangle_y = \frac{1}{\sqrt{2}}(|0\rangle + i|1\rangle)$ is an eigenvector of σ_y with eigenvalue +1. The former is an eigenstate of the interaction term in the Floquet operator \mathcal{U} , while the latter is the eigenstate of the field. When $|++\rangle_y$ is the initial state, its evolution lies entirely in the positive-parity sector as it can be also written as $\otimes^3 |+\rangle_y = (|\phi_1^+\rangle + \sqrt{3}i|\phi_2^+\rangle)/2$. As a coherent state it corresponds to being localized at $|\pi/2, -\pi/2\rangle$. The corresponding classical object is a fixed point that is stable until $\kappa_0 = 2$. The time-evolved state is then

$$|\psi_n\rangle = \mathcal{U}^n |++\rangle_y = e^{-in(\frac{\pi}{4} + \kappa)} (\gamma_n |\phi_1^+\rangle + \delta_n |\phi_2^+\rangle), \quad (35)$$

where $\gamma_n = (\alpha_n - i\sqrt{3}\beta_n^*)/2$ and $\delta_n = (\beta_n + i\sqrt{3}\alpha_n^*)/2$, and the α_n and β_n are same as in Eq. (13).

One can obtain the single-party reduced state by tracing out any two qubits,

$$\rho_1(n) = \begin{Bmatrix} \frac{1}{2} & -\frac{i}{3} [|\delta_n|^2 - \sqrt{3} \text{Im}(\gamma_n \delta_n^*)] \\ \frac{i}{3} [|\delta_n|^2 - \sqrt{3} \text{Im}(\gamma_n \delta_n^*)] & \frac{1}{2} \end{Bmatrix}. \quad (36)$$

The eigenvalues of $\rho_1(n)$ are simple and given by $2\chi^2 U_{n-1}^2(\chi)$ and $1 - 2\chi^2 U_{n-1}^2(\chi)$; hence the linear entropy is

$$S_{(\frac{\pi}{2}, -\frac{\pi}{2})}^{(3)}(n, \kappa_0) = 4\chi^2 U_{n-1}^2(\chi) [1 - 2\chi^2 U_{n-1}^2(\chi)]. \quad (37)$$

Figure 6 shows the growth of the entanglement entropy in this state as a function of time n for four different values of κ_0 . Comparing with Fig. 3 we see that the entanglement increases much more slowly, in keeping with the classical interpretation of this state as being localized on a fixed point. However, the initial $n = 1$ is the same in both the cases, $S_{(\frac{\pi}{2}, -\frac{\pi}{2})}^{(3)}(1, \kappa_0)$ is still given Eq. (22), and hence the entanglement after the first step is $\sim \kappa_0^2/9$ for small κ_0 .

A difference is seen at $n = 2$ when

$$S_{(\frac{\pi}{2}, -\frac{\pi}{2})}^{(3)}(2, \kappa_0) = \sin^4(\kappa_0/3) [1 - \frac{1}{2} \sin^4(\kappa_0/3)], \quad (38)$$

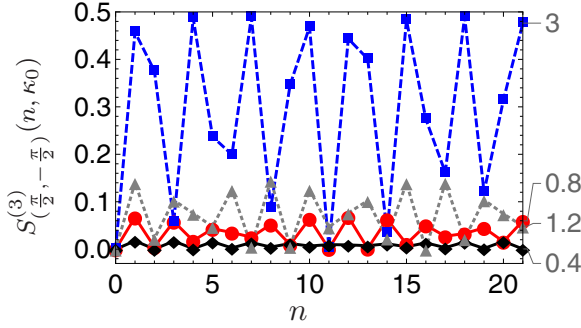


FIG. 6. Linear entropy of a single-qubit reduced state versus n is plotted for different values of κ_0 . Curves correspond to $\kappa_0 = 0.4, 0.8, 1.2,$ and 3.0 are shown by a solid line with diamonds, a solid line with circles, a dashed line with triangles, and a dashed line with squares, respectively.

thus while $S_{(0,0)}^{(3)}(2, \kappa_0) = S_{(0,0)}^{(3)}(1, \kappa_0)$, $S_{(\pi/2, -\pi/2)}^{(3)}(2, \kappa_0) < S_{(\pi/2, -\pi/2)}^{(3)}(1, \kappa_0)$. In fact, the contrast with the state $|000\rangle$ is most apparent when we observe that Eq. (37) implies that

$$S_{(\pi/2, -\pi/2)}^{(3)}(n, \kappa_0) \leq 4\chi^2 U_{n-1}^2(\chi) \leq \frac{4}{3} \sin^2(\kappa_0/3), \quad (39)$$

the last inequality is due to the upper bound $|U_{n-1}(\chi)| \leq 2/\sqrt{3}$ which as has been observed above holds due to the restriction $|\chi| \leq 1/2$. This inequality is useful for small κ_0 in which case we have that $S_{(\pi/2, -\pi/2)}^{(3)}(n, \kappa_0) \leq 4\kappa_0^2/27$ and is hence very close to the entanglement produced at the very first step, namely $\kappa_0^2/9$, and in particular has no secular growth toward large entanglement.

The long-time average value of the linear entropy is calculated exactly as the case when the initial state was $|000\rangle$, and we therefore merely display the result

$$\langle S_{(\pi/2, -\pi/2)}^{(3)}(\kappa_0) \rangle = \frac{\sin^2(\kappa_0/3)}{[4 - \sin^2(\kappa_0/3)]^2} [8 - 5 \sin^2(\kappa_0/3)]. \quad (40)$$

The major difference between the two initial states considered so far is apparent in this formula, as it is smooth at $\kappa_0 = 0$ and vanishes at $\kappa_0 = 0$, unlike Eq. (29). The fact that the classical orbit in this case is a fixed point as opposed to a period-4 orbit is notable. In the case of the state $|000\rangle$, extremely nonclassical states such as the GHZ can form at sufficiently long times and leads to the large average. We will see that the state centered at the fixed point can also have a large nonzero average for the case of four qubits, again due to the formation of highly nonclassical states mediated by tunneling.

Figure 7 shows the long-time average $\langle S_{(\theta_0, \phi_0)}^{(3)}(\kappa_0) \rangle$ as a function of κ_0 , for the case of three qubits, and three initial states, two of them being what we just discussed, namely $|000\rangle$ and $|++\rangle_y$, which correspond to the cases with $\theta_0 = 0$ and $\pi/2$, respectively. That they are in some sense extreme cases is seen clearly in this figure. Each is seen to increase with the torsion κ_0 to $1/3$, while a state with $\theta_0 = \pi/4$ (and in all cases $\phi_0 = -\pi/2$) grows to $7/24$ which we will see is the lowest for any state. The average value of the linear entropy in the N -qubit permutation symmetric subspace

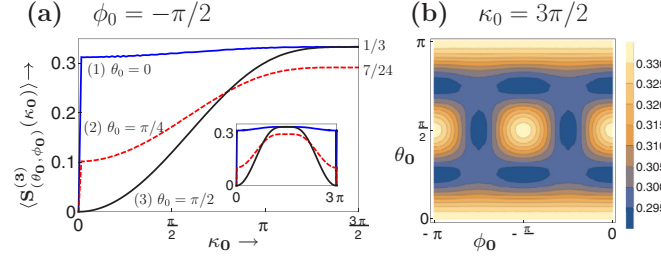


FIG. 7. (a) Time-averaged linear entropy, obtained over $n = 1000$ periods, of a single qubit vs. the parameter κ_0 , for three initial coherent states $|\theta_0, \phi_0\rangle$. The Eqs. (29) and (40) apply to the curves labeled (1) and (3), as for $\theta_0 = 0$ the value of ϕ_0 is immaterial on the sphere. Inset shows the entanglement periodicity in the parameter at $\kappa_0 = 3\pi$. Part (b) displays the time-averaged linear entropy across all initial coherent states for the value $\kappa_0 = 3\pi/2$ and is described by Eq. (42).

[60] is given by

$$S_{\text{RMT}}(N) = \frac{N-1}{2N}, \quad (41)$$

and for $N = 3$ this also gives $1/3$. For at least three particular initial states, with important classical phase-space correspondences, $|0, 0\rangle \equiv |000\rangle$ and $|\pi/2, \pm\pi/2\rangle \equiv |\pm\pm\pm\rangle_y$, this value is, remarkably, exactly attained for $\kappa_0 = 3\pi/2$, as easily verified from Eqs. (29) and (40). Thus ergodicity is attained as time-averaged linear entropy approaches the state-space-averaged linear entropy.

Note that the $j = \infty$, classical system shows a transition to chaos in the same range of the parameter. While $j = 3/2$ is too small to see effects such as the fixed points' loss of stability, the overall region surrounding the classical fixed points $(\theta_0, \phi_0) = (\pi/2, \pm\pi/2)$ being stable for small κ_0 and gradually losing stability as the parameter is increased is reflected in the gradual increase of average entropy corresponding to the initial states $|\pi/2, \pm\pi/2\rangle$ starting from 0 when $\kappa_0 = 0$. Notice that from a purely quantum mechanical view, $\otimes^2 j|\pm\rangle_y$ are eigenstates of \mathcal{U} at $\kappa_0 = 0$. In contrast, the initial state $|000\rangle$ corresponds to a classical period-4 orbit and assumes entanglement entropy as large as $5/16$ for arbitrarily small κ_0 .

Arbitrary initial states, $\kappa_0 = 3\pi/2$

For the three-qubit case, the case of $\kappa_0 = 3\pi/2$ is an extreme one, and the eigenvalues of \mathcal{U} in this case are $\exp(\pm 2\pi i/3)$ and $\pm \exp(\pm \pi i/6)$, implying that $\mathcal{U}^{12} = I$. Thus infinite time averages are finite ones over a period; in fact, entanglement has a period of 6 in this case and for arbitrary initial coherent states, the time-averaged entanglement entropy is obtained via a straightforward, if long, computation whose details we skip and state the result as

$$\langle S_{(\theta_0, \phi_0)}^{(3)}(3\pi/2) \rangle = \frac{1}{48} \{15 + \cos(4\theta_0) + [1 + 3 \cos(2\theta_0)] \sin^4 \theta_0 \sin^2(2\phi_0)\}. \quad (42)$$

This takes values in the narrow interval $[7/24, 1/3]$, and is shown in Fig. 7. The minimum corresponds to several initial states including $|\pi/4, \pm\pi/2\rangle$ and the maximum includes the

$|0, 0\rangle$ and $|\pi/2, \pm\pi/2\rangle$ states as already noted above. The structures seen are not directly linked to classical phase-space orbits, except through shared symmetries [49], and cannot be expected to do so as the classical limit is for fixed κ_0 and $j \rightarrow \infty$. Nevertheless, these results lend quantitative credence to thermalization in the sense that the time-averaged entropy of subsystems of most states are close to the ensemble average for suitable large κ_0 , even for the three-qubit case [15,18], which, when $\kappa_0 = 3\pi/2$, approaches $1/3$. Coincidentally, as mentioned above, this is same as the average linear entropy of a single-qubit reduced state in a set of random symmetric three-qubit states. The calculations for the case of a general initial state and more figures of the long-time averages are presented in the Appendix.

III. COMPARISON WITH AN EXPERIMENT

We analyze the data from a recent experiment [15] that demonstrates the kicked top dynamics of a spin-3/2, using three superconducting transmon qubits. Experimental data correspond to the two special initial states: $|0, 0\rangle$ and $|\pi/2, -\pi/2\rangle$ (whose analytical solutions are given in Secs. II A and II B, respectively), each one for two values of chaoticity parameter, $\kappa_0 = 0.5$ and 2.5 . A three-qubit state is experimentally initialized in given initial states (respectively) and then allowed to undergo a series of kicks and evolutions, separately for $\kappa_0 = 0.5$ and 2.5 , as described in Ref. [15] for a total of 20 time steps.

Details of the analysis of the raw experimental data, which often has negative states, is outlined. We analyzed the complete quantum state tomographic data, obtained at the end of each time step. The state of a three-qubit system is obtained via complete quantum state tomography using a set of 64 projective measurements. These projective measurements are constructed by taking the combinations of Pauli- x, y, z matrices ($\sigma_x, \sigma_y, \sigma_z$) and the identity operator (I) [15,61]. These measurements are experimentally realized by various single-qubit rotations (\mathcal{R}) followed by σ_z measurements on individual qubits that effectively performs a $\sigma_{i'}$ measurement [for $i' = x, \mathcal{R} = \text{Hadamard operator } (H_d)$; $i' = y, \mathcal{R} = S \cdot H_d$ where S is phase shift operator; $i' = z, \mathcal{R} = I$] [15]. Multiple implementations of each measurement provides the relative occupancy of the eight basis states of a three-qubit system. The resulting relative populations (p_m) of these eight states are thus obtained experimentally.

In order to compensate the effect of errors induced by the measurements, the intrinsic populations (p_{int}) are obtained via a correction matrix (F) [62,63]. We have $p_{\text{int}} = F^{-1}p_m$, where $F = F_1 \otimes F_2 \otimes F_3$. F_i is the measurement error corresponding to i th qubit, given as

$$F_i = \begin{bmatrix} f_0^{(i)} & 1 - f_1^{(i)} \\ 1 - f_0^{(i)} & f_1^{(i)} \end{bmatrix}.$$

Here $f_0^{(i)}$ is the probability by which a state $|0\rangle$ of the i th qubit is correctly identified as $|0\rangle$, while $1 - f_1^{(i)}$ is the probability by which, a state that is actually $|0\rangle$ is being wrongly considered as $|1\rangle$. $f_0^{(i)}$ and $f_1^{(i)}$ are termed as the measurement fidelities of the basis states $|0\rangle$ and $|1\rangle$, respectively, of the i th qubit. Using a part of the measurement data

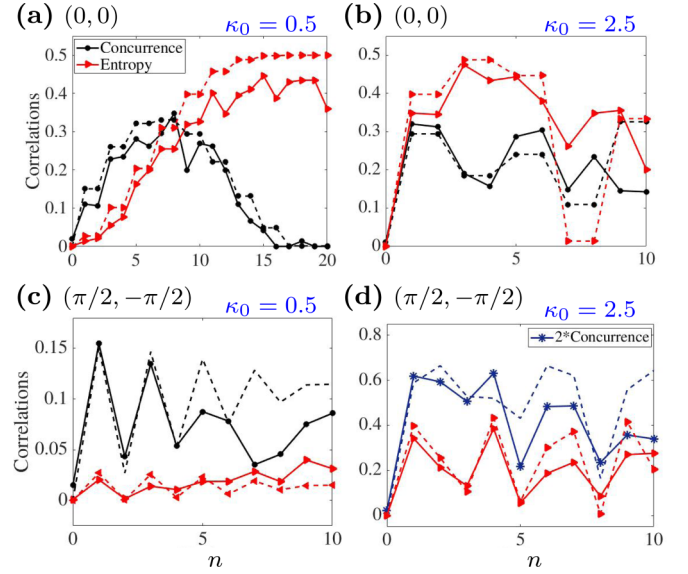


FIG. 8. Plots showing analytical (dashed curves with markers), experimental (solid curves with markers), and numerical (dashed) curves of linear entropy and concurrence as a function of the number of kicks, as the initial state $|\psi_0\rangle$ is evolved under repeated applications of operator \mathcal{U} . Parameters of the initial state, (θ_0, ϕ_0) , and chaoticity parameter, κ_0 , are specified in each figure. Analytical (wherever plotted) and numerical curves exactly overlap and hence cannot be seen separately.

corresponding to the initial state preparation, we estimated the measurement fidelities as $f_0^{(1)} = 0.98$, $f_1^{(1)} = 0.92$, $f_0^{(2)} = 0.98$, $f_1^{(2)} = 0.94$, $f_0^{(3)} = 0.96$, and $f_1^{(3)} = 0.87$. The intrinsic populations obtained in this manner are positive (as observed to a second decimal place). Using these intrinsic population values, three-qubit density operators are obtained that further undergo the convex optimization. The fidelities between the theoretically expected (ρ_t) and the experimentally obtained (ρ_e) states is given by [15]

$$\mathcal{F} = \text{Tr} \sqrt{\sqrt{\rho_t} \rho_e \sqrt{\rho_t}}. \quad (43)$$

These experimentally obtained three-qubit density operators are then used in our study to obtain the correlations, such as linear entropy of a single-qubit reduced state and a two-qubit entanglement measure, concurrence.

Experimental data has its own imperfections, and the three-qubit experimental state may not be permutation symmetric under qubit exchange. Therefore, corresponding to each three-qubit density operator, three single-qubit reduced-density operators (say, ρ_1, ρ_2, ρ_3), and three two-qubit reduced-density operators (say, $\rho_{12}, \rho_{23}, \rho_{13}$) are obtained. At each time step, using various single-qubit and two-qubit density operators correlations such as linear entropy and concurrence are calculated, respectively, and their average behavior is observed.

Figure 8 shows the comparison between the analytical results (dashed curves with markers) and those using experimental data from Ref. [15], shown as solid curves with markers for $\kappa_0 = 0.5$ and 2.5 . Numerical results are also plotted as dashed curves in Fig. 8 but are naturally indistinct from the respective analytical results. More extensive analytical results

have already been displayed in Figs. 3–6 and discussed in the previous section.

Figures 8(a) and 8(b), corresponds to the initial state $|000\rangle$, whose classical limit is the period-4 orbit. This classical the period-4 orbit is unstable at $\kappa_0 = 2.5$ and we see a rapid growth in the entanglement. However, even at $\kappa_0 = 0.5$ entanglement grows to near-maximal values, consistent with the large time average in Eq. (29) and with the analysis that predicts that the maximum occurs at a timescale $n_* \sim 3\pi/\kappa_0 \sim 19$. We also noted that the entanglement at time $2n$ is same as the entanglement at time $2n - 1$, see Eqs. (21) and (33). Interestingly these are quite remarkably present (but previously unnoticed) in the experimental data for the first few time steps. All entanglement properties including concurrence is left approximately unchanged in the experimental data for an odd-to-even time step as seen in Figs. 8(a) and 8(b). The degradation of this phenomenon is naturally to be attributed to decoherence and maybe a good measure of it.

The plots showing comparison of linear entropy and concurrence from the experimental data for the state $|\pi/2, -\pi/2\rangle$ when $\kappa_0 = 0.5$ and $\kappa_0 = 2.5$ are shown in Figs. 8(c) and 8(d). It shows a much smaller entropy growth for $\kappa_0 = 0.5$ in comparison to the state $|000\rangle$, consistent with the bound in Eq. (39) and is a reflection, in the semiclassical limit, of the stable neighborhood of $|\pi/2, -\pi/2\rangle$. This is also consistent with the long-time average, already displayed in Eq. (40). More qualitative discussions of the time evolution have been published in Ref. [34].

IV. EXACT SOLUTION FOR FOUR-QUBITS

It is particularly interesting to study a four-qubit kicked top as this is the smallest system where all-to-all interaction among qubits is different from that of nearest-neighbor interaction and therefore presents a special case of a genuinely nonintegrable system. Surprisingly, even in this case, an exact solution to the kicked top with spin $j = 2$, is possible. Similarly to that of three-qubit kicked top, we are again confined to $(2j + 1 = 5)$ -dimensional permutation symmetric subspace of the total $2^{2j} = 16$ -dimensional Hilbert space. In this case the parity symmetry reduced and permutation symmetric basis in which \mathcal{U} is block-diagonal is

$$\begin{aligned} |\phi_1^\pm\rangle &= \frac{1}{\sqrt{2}}(|W\rangle \mp |\bar{W}\rangle), \\ |\phi_2^\pm\rangle &= \frac{1}{\sqrt{2}}(|0000\rangle \pm |1111\rangle), \quad \text{and} \\ |\phi_3^\pm\rangle &= \frac{1}{\sqrt{6}} \sum_{\mathcal{P}} |0011\rangle_{\mathcal{P}}, \end{aligned} \quad (44)$$

where $|W\rangle = \frac{1}{2} \sum_{\mathcal{P}} |0001\rangle_{\mathcal{P}}$, $|\bar{W}\rangle = \frac{1}{2} \sum_{\mathcal{P}} |1110\rangle_{\mathcal{P}}$, and $\sum_{\mathcal{P}}$ sums over all possible permutations. Husimi plots for each of these states is shown in Fig. 9. While all of these states $|\phi_j^\pm\rangle$ are eigenstates of the parity operator $\otimes_{j=1}^4 \sigma_j^y$ with eigenvalue ± 1 , a peculiarity of four qubits is that $|\phi_1^\pm\rangle$ is also an eigenstate of the Floquet operator \mathcal{U} with eigenvalue -1 for all values of the parameter κ_0 .

Thus the five-dimensional space splits into $1 \oplus 2 \oplus 2$ subspaces on which the operators are $\mathcal{U}_0 = -1$ and \mathcal{U}_{\pm} . Note that

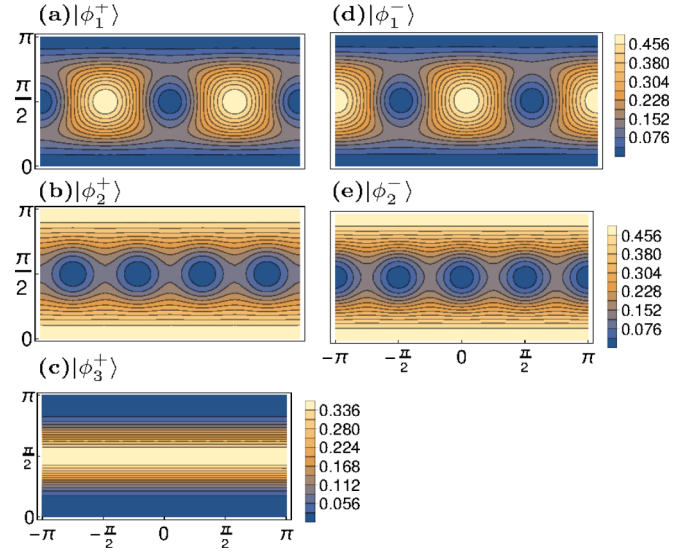


FIG. 9. Husimi (quasiprobability distribution, $|\langle \phi_i | \phi_0, \theta_0 \rangle|^2$) plots for a set of 5 four-qubit bases states ($|\phi_i\rangle$), where $|\theta_0, \phi_0\rangle$ is an arbitrary four-qubit, parametrized by (θ_0, ϕ_0) .

we continue to use the same symbol for the symmetry-reduced Floquet operators as for the three-qubit case, although they are not the same. It is interesting that the eigenstate $|\phi_1^\pm\rangle$ still has a classically viable interpretation but only for small κ_0 , where, as is clear from the Husimi, it is localized on the fixed points and the symmetric islands. A more detailed study of eigenstates is postponed while we concentrate here on the time evolution.

In this basis, the unitary Floquet operator \mathcal{U} becomes block diagonal, which makes it easy to take the n th power of the unitary operator \mathcal{U} ,

$$\mathcal{U}^n = \begin{bmatrix} (-1)^n & 0 & 0 \\ 0 & \mathcal{U}_+^n & 0 \\ 0 & 0 & \mathcal{U}_-^n \end{bmatrix}. \quad (45)$$

Thus in this case also we do not encounter the need to take powers of any matrix other than two-dimensional ones. Block \mathcal{U}_+ is \mathcal{U} in the basis $\{\phi_2^+, \phi_3^+\}$ and is

$$\mathcal{U}_+ = -ie^{-\frac{ik}{2}} \begin{pmatrix} \frac{i}{2}e^{-ik} & \frac{\sqrt{3}i}{2}e^{-ik} \\ \frac{\sqrt{3}i}{2}e^{ik} & -\frac{i}{2}e^{ik} \end{pmatrix}, \quad (46)$$

while \mathcal{U}_- is \mathcal{U} in the basis $\{\phi_1^-, \phi_2^-\}$,

$$\mathcal{U}_- = e^{-\frac{3ik}{4}} \begin{pmatrix} 0 & e^{\frac{3ik}{4}} \\ -e^{-\frac{3ik}{4}} & 0 \end{pmatrix}, \quad (47)$$

where for simplicity we have used $\kappa = \kappa_0/2$.

Adopting the same procedure as for the case of 3 qubits, namely expressing \mathcal{U}_+ as a $SU(2)$ rotation, apart from a phase, and taking its power results in

$$\mathcal{U}_+^n = e^{-\frac{in(\pi+\kappa)}{2}} \begin{pmatrix} \alpha_n & i\beta_n^* \\ i\beta_n & \alpha_n^* \end{pmatrix}, \quad (48)$$

where

$$\alpha_n = T_n(\chi) + \frac{i}{2}U_{n-1}(\chi)\cos\kappa, \quad \beta_n = \frac{\sqrt{3}}{2}U_{n-1}(\chi)e^{i\kappa}. \quad (49)$$

As above, $T_n(\chi)$ and $U_{n-1}(\chi)$ denote the Chebyshev polynomials of the first and second kinds, respectively, but now $\chi = \sin\kappa/2 = \sin(\kappa_0/2)/2$.

Similarly,

$$\mathcal{U}_-^n = e^{-\frac{3i\kappa}{4}} \begin{pmatrix} \cos\frac{n\pi}{2} & e^{\frac{3i\kappa}{4}}\sin\frac{n\pi}{2} \\ -e^{-\frac{3i\kappa}{4}}\sin\frac{n\pi}{2} & \cos\frac{n\pi}{2} \end{pmatrix}, \quad (50)$$

which has a much simpler form than the \mathcal{U}_+^n and in fact $\mathcal{U}_-^2 = -e^{-3i\kappa/4}I_2$ is up to a dynamical phase proportional to the identity. Thus all states in the negative-parity subspace are essentially periodic with period 2, a uniquely quantum feature. In particular, the GHZ state $|\phi_2^-\rangle = (|0000\rangle - |1111\rangle)/\sqrt{2}$ would be of this kind. Using these it is possible to find the exact evolution of the entanglement entropy of any one qubit and again in particular we again concentrate on the initial states being $|0000\rangle$ and $|\pm\pm\pm\pm\rangle_y$, for the same reasons as in the three-qubit case.

A. Initial state $|\psi_0\rangle = |0000\rangle$

Considering four-qubit state $|0000\rangle$, under the “ n ” implementations of unitary operator \mathcal{U} ,

$$\mathcal{U}^n|0000\rangle = \frac{1}{\sqrt{2}}(\mathcal{U}_+^n|\phi_2^+\rangle + \mathcal{U}_-^n|\phi_2^-\rangle), \quad (51)$$

leads to the state $|\psi_n\rangle$ at time n . Just as for the three-qubit case the state $\mathcal{U}^{2n}|0000\rangle$ is to local-unitary operators same as $\mathcal{U}^{2n-1}|0000\rangle$, and therefore again all entanglement properties have “steps” in their dynamical evolution and it is sufficient to consider the time n to be an even integer. In this case,

$$|\psi_n\rangle = e^{-\frac{i\pi(n+\kappa)}{2}} \frac{1}{\sqrt{2}}(\alpha_n|\phi_2^+\rangle + i\beta_n|\phi_3^+\rangle + e^{-\frac{i\kappa}{4}}|\phi_2^-\rangle). \quad (52)$$

Single-qubit reduced-density matrix is simply diagonal for even values of n , eigenvalues being $\lambda(n, \kappa_0)$ and $1 - \lambda(n, \kappa_0)$, where $\lambda(n, \kappa_0) = \frac{1}{2}[1 + \xi_n(\kappa_0)]$, where

$$\begin{aligned} \xi_n(\kappa_0) &= \text{Re}(\alpha_n e^{in\kappa_0/8}) \\ &= T_n(\chi) \cos\frac{n\kappa_0}{8} - \frac{1}{2}U_{n-1}(\chi) \cos\frac{\kappa_0}{2} \sin\frac{n\kappa_0}{8}. \end{aligned} \quad (53)$$

For even values of n , linear entropy of a single-qubit reduced state is given by

$$S_{(0,0)}^{(4)}(n, \kappa_0) = \frac{1}{2}[1 - \xi_n^2(\kappa_0)], \quad (54)$$

and at odd values $S_{(0,0)}^{(4)}(2n-1, \kappa_0) = S_{(0,0)}^{(4)}(2n, \kappa_0)$. Figure 10 shows the evolution of this entanglement entropy for a few representative values of κ_0 . In particular, even for $n=2$ (which is the same as $n=1$), we get a fairly long expression for the entanglement entropy; hence rather than display it, we state that for small κ_0 it increases as $S_{(0,0)}^{(4)}(1, \kappa_0) \approx 3\kappa_0^2/32$, which is very similar to the corresponding three-qubit case. It grows monotonically with κ_0 until $\kappa_0 = \pi$ where it attains the upper bound of $1/2$ already, in contrast to the three-qubit case which attains this only at $\kappa_0 = 3\pi/2$.

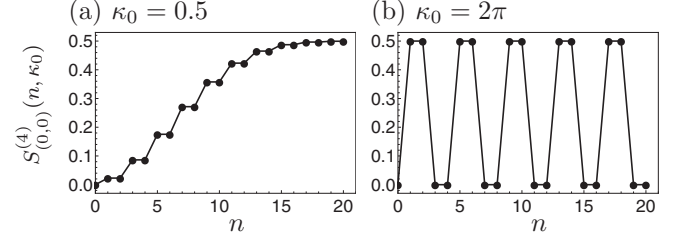


FIG. 10. Linear entropy of a single-qubit reduced state versus n is plotted at different values of κ_0 shown in parts (a) and (b), corresponding to a four-qubit initial state, $|0000\rangle$.

To find the relevant timescales in the growth of the entanglement, we note that the maximum value of the entropy is attained when $\xi_n(\kappa_0) = 0$. From Eq. (53), and noting that the zeros of $T_n(\chi)$ and $U_{n-1}(\chi)$ do not occur simultaneously, we first examine the case when n is even and $U_{n-1}(\chi)$ vanishes. This is similar to the analysis of the three-qubit case above and we simply state that this implies that $n_* \approx 4\pi/\kappa_0$. Thus the first even time at which the second half of Eq. (53) vanishes is n_* ; however, if this condition is satisfied the first part also vanishes as the $\cos(n\kappa_0/8)$ does. Thus the typical timescale for the large entanglement to develop is slightly larger than the case of three qubits where it was $3\pi/\kappa_0$. At the time when the entanglement is maximum, $\beta_n \approx 0$ and the resultant states are superpositions of $|\phi_2^\pm\rangle$ and are GHZ states. Thus the large one-qubit entanglement observed in the experiment in Ref. [15] for $\kappa_0 = 0.5$ has more to do with the creation of such GHZ states than thermalization or chaos.

Long-time average of the linear entropy is obtained by averaging over the time n and is given by

$$\langle S_{(0,0)}^{(4)}(\kappa_0) \rangle = \frac{1}{8} \left[\frac{9 + 2\cos^2(\kappa_0/2)}{3 + \cos^2(\kappa_0/2)} \right], \quad \kappa_0 \neq 0, 2\pi. \quad (55)$$

For $\kappa_0 = 0$, or 2π , the entanglement vanishes. As soon as κ_0 becomes nonzero, this long-time-averaged linear entropy attains a value of $2.75/8$, which further increases with κ_0 and attains a maximum value of $3/8$ at $\kappa_0 = \pi$, as shown by the dashed curve in Fig. 11.

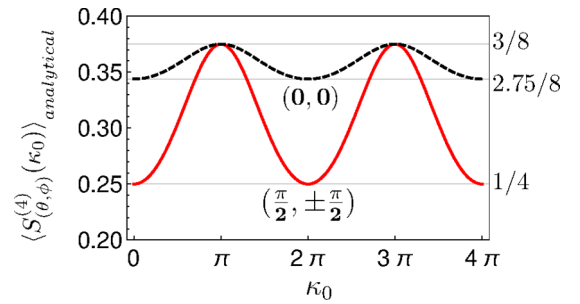


FIG. 11. Analytically obtained expressions for time-averaged linear entropy for initial states $|0000\rangle$ [Eq. (55)] and $|++++\rangle_y$ [Eq. (59)] are plotted for $\kappa_0 \in (0, 4\pi)$. Extreme values are presented as horizontal lines, with their respective values $S_{(\theta, \phi)}^{(4)}(\kappa_0) = \text{constant}$ specified on the right side. Solid red curve and dashed black curve correspond to initial states $|++++\rangle_y$ and $|0000\rangle$, respectively.

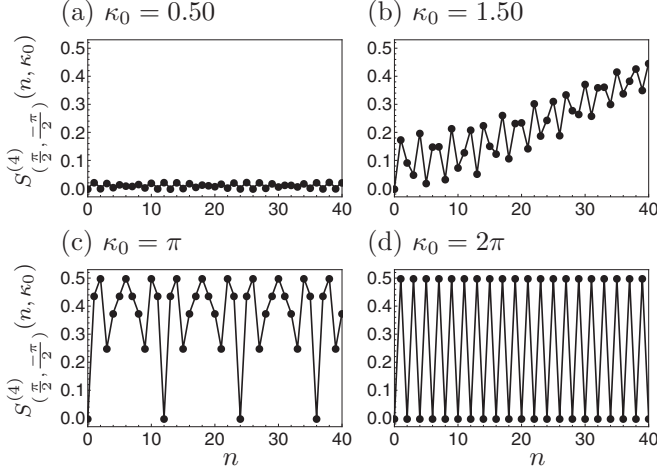


FIG. 12. Linear entropy of a single-qubit reduced state versus n is plotted at different values of κ_0 shown in parts (a), (b), (c), and (d), corresponding to a four-qubit initial state, $|++++\rangle_y$.

Thus, in this case, long-time-averaged linear entropy of a single-qubit reduced state oscillates within a very small interval of range $1/32$ for $\kappa_0 \in (0, 2\pi)$.

B. Initial state $|\psi_0\rangle = |++++\rangle_y$

This state lies entirely in the positive-parity subspace of the five-dimensional permutation symmetric space of four qubits and is given by

$$\otimes^4|+\rangle_y = \frac{i}{\sqrt{2}}|\phi_1^+\rangle + \frac{1}{\sqrt{8}}|\phi_2^+\rangle - \sqrt{\frac{3}{8}}|\phi_3^+\rangle, \quad (56)$$

which under the action of \mathcal{U}^n leads to $|\psi_n\rangle = \mathcal{U}_+^n|++++\rangle_y$, such that (for $n > 1$)

$$|\psi_n\rangle = \frac{(-1)^n}{\sqrt{2}}[i|\phi_1^+\rangle + e^{i\delta}(\alpha_n/2 - i\sqrt{3}\beta_n^*/2)|\phi_2^+\rangle - e^{i\delta}(\sqrt{3}\alpha_n^*/2 - i\beta_n/2)|\phi_3^+\rangle], \quad (57)$$

where $\delta = n(2\pi - \kappa_0)/4$. The reduced-density matrix of any one of the four qubits is given by

$$\rho_1(n, \kappa_0) = \text{Tr}_{2,3,4}(|\psi_n\rangle\langle\psi_n|) = \begin{bmatrix} 1/2 & \xi'_n(\kappa_0) \\ \xi'_n(\kappa_0)^* & 1/2 \end{bmatrix}, \quad (58)$$

where

$$\xi'_n(\kappa_0) = -i[T_n(\chi)\cos\delta + U_{n-1}(\chi)\sin\delta\cos(\kappa_0/2)],$$

and the linear entropy is given by

$$S_{(\pi/2, -\pi/2)}^{(4)}(n, \kappa_0) = \frac{1}{2}[1 - |\xi'_n(\kappa_0)|^2].$$

Figure 12 shows the evolution of this entanglement entropy for a few representative values of κ_0 .

A closed form expression for long-time-average linear entropy is then obtained as for the other case and results in (for $\kappa_0 \neq 0, 2\pi$),

$$\langle S_{(\pi/2, \pm\pi/2)}^{(4)} \rangle = \frac{1}{8} \left[\frac{9 - \cos^2(\kappa_0/2)}{3 + \cos^2(\kappa_0/2)} \right]. \quad (59)$$

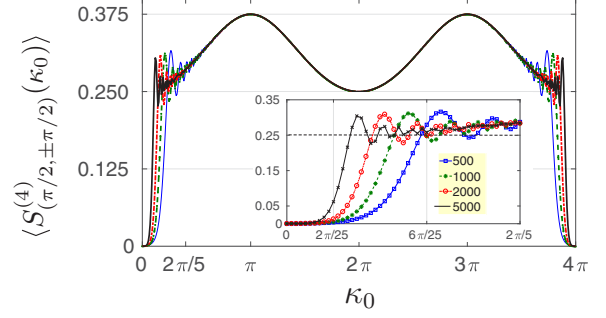


FIG. 13. Simulated time-average linear entropy $[\langle S_{(\pi/2, \pm\pi/2)}^{(4)}(\kappa_0) \rangle]$ subject to initial state, $|(\pi/2, \pm\pi/2)\rangle$, plotted versus κ_0 , is shown for different values of n (as given in the inset) in the interval $\kappa_0 \in [0, 4\pi]$. Inset shows the blown-up horizontal scale for $\kappa_0 \in [0, \Delta\kappa_0]$, where $\Delta\kappa_0 = 2\pi/5$, that clearly presents the curves approaching the solid curve of Fig. 11.

As soon as κ_0 becomes nonzero, this long-time-averaged linear entropy attains its minimum value of $1/4$, which further increases with κ_0 and attains a maximum value of $3/8$ at $\kappa_0 = \pi$, as shown by the solid red curve in Fig. 11. In this case, long-time-averaged linear entropy of single-qubit reduced state oscillates within a relatively larger interval of range $1/8$ for $\kappa_0 \in (0, 4\pi)$.

Time-averaged linear entropy of single-qubit reduced state in both of these cases reach their maximum value of $3/8$ when $\kappa_0 = \pi$ and, remarkably, this matches with the average from the ensemble of random permutation symmetric states [60] of four qubits $S_{\text{RMT}}(4)$ as in the case of the three-qubit case. In addition we see that the average for the states at $(\pi/2, \pm\pi/2)$ attain the value of $1/4$ for arbitrarily small κ_0 in contrast to the three-qubit case which vanishes as in Eq. (40). In fact, the nonzero average is seen in numerical calculations to be attained only on averaging over extremely long times for small κ_0 , shown in Fig. 13, where different curves correspond to time average over different times (as labeled in terms of n in the inset). For small values of κ_0 , i.e., $\kappa_0 = 2p\pi \pm \Delta\kappa_0$ (p being an integer), time-average behavior of linear entropy for different times does not converge and approaches the infinite-time average consistent with Eq. (59) and Fig. 11, as $n \rightarrow \infty$. This slow thermalization, specifically for state $|(\pi/2, \pm\pi/2)\rangle$, is attributed to the process of dynamical tunneling to which we now turn.

C. Dynamical tunneling

This very slow process is due to tunneling between $\otimes^4|+\rangle_y$ and $\otimes^4|-\rangle_y$. At $\kappa_0 = 0$, two positive-parity eigenvectors of \mathcal{U} , $|\phi_1^+\rangle$, and $|\phi_{23}^+\rangle = \frac{1}{2}|\phi_2^+\rangle - \frac{\sqrt{3}}{2}|\phi_3^+\rangle$ are degenerate with eigenvalue -1 . These can also be written as four-qubit GHZ states [64,65]:

$$i|\phi_1^+\rangle = (\otimes^4|+\rangle_y - \otimes^4|-\rangle_y)/\sqrt{2}, \quad (60)$$

the unchanging eigenstate and

$$|\phi_{23}\rangle = (\otimes^4|+\rangle_y + \otimes^4|-\rangle_y)/\sqrt{2}. \quad (61)$$

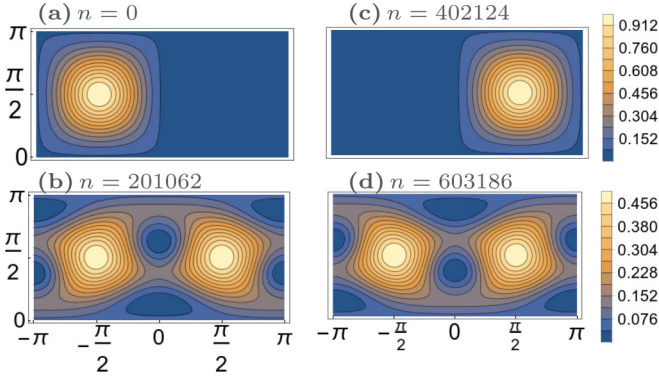


FIG. 14. Husimi (quasiprobability distribution) plots for the four-qubit initial state, $\otimes^4|+\rangle$, evolving under n implementations of \mathcal{U} , and leading to tunneling to the state, $\otimes^4|-\rangle$, at time $n_* \approx 128\pi/\kappa_0^3 \approx 402124$ ($\kappa_0 = 0.1$).

Thus,

$$\mathcal{U}^n \otimes^4 |+\rangle_y = (-1)^n \frac{i}{\sqrt{2}} |\phi_1^+\rangle + \mathcal{U}_+^n \frac{1}{\sqrt{2}} |\phi_{23}^+\rangle. \quad (62)$$

The eigenvalue of \mathcal{U}_+ , that is, -1 at $\kappa_0 = 0$, is $e^{i\gamma_-}$ with

$$\gamma_- = \frac{\kappa_0}{4} + \pi - \sin^{-1} \left(\frac{1}{2} \sin \frac{\kappa_0}{2} \right) \approx \pi - \frac{\kappa_0^3}{128}. \quad (63)$$

This implies that for $\kappa_0 \ll 1$, the corresponding state and $|\phi_1^+\rangle$ are nearly degenerate. The splitting leads to a change in the relative phase of their contributions in Eq. (62) and at time $n_* \approx 128\pi/\kappa_0^3$ the evolved state is close to $\otimes^4|-\rangle$, leading to tunneling as shown in Fig. 14 between what in the classical limit are two stable islands. At time $n = n_*/2$ the state obtained is close to the GHZ state $(\otimes^4|+\rangle_y - i \otimes^4|-\rangle_y)/\sqrt{2}$.

This tunneling is observed whenever $\otimes^{2j}|\pm\rangle$ are degenerate eigenstates of the rotation part of the Floquet \mathcal{U} . This implies that the number of qubits should be an integer multiple of $2\pi/p$, where p is the rotation angle (we have used $p = \pi/2$ and hence the tunneling occurs when the number of qubits is a multiple of 4).

For larger number of qubits, the average single-qubit entropy, normalized by the random state average, is numerically found when the initial state is $\otimes^{2j}|+\rangle_y$ and shown in Fig. 15. The number of qubits used for the cases shown in this figure

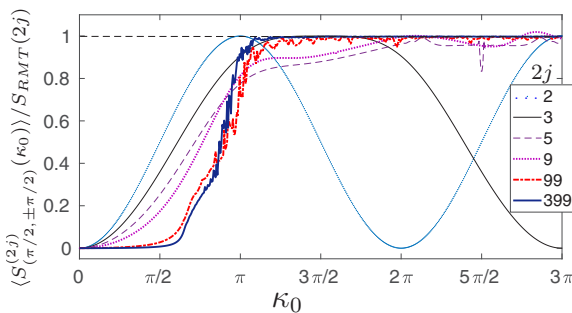


FIG. 15. Normalized average single-qubit entanglement when the initial state is $\otimes^{2j}|+\rangle_y$ for increasing number of qubits (except multiples of 4 where there is tunneling for $p = \pi/2$).

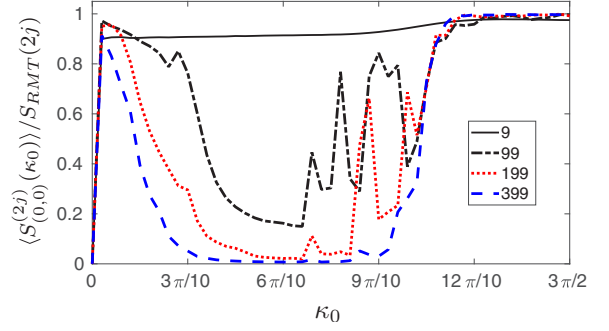


FIG. 16. Normalized average single-qubit entanglement when the initial state is $\otimes^{2j}|0\rangle$ for increasing number of qubits.

are not multiples of 4, and hence the long-time average vanishes at $\kappa_0 = 0$, that is there is no tunneling. The trend is in keeping with a more complex classical phase space that becomes fully chaotic when the random state average is approached. The initial state being centered on a fixed point, increasing the number of qubits leads to a sharp growth beyond $\kappa_0 = 2$ when the fixed point becomes unstable, and a more detailed study of this is found in Ref. [13], without the connection to tunneling. Interestingly even for the three-qubit case, for which we have the analytical evaluation in Eqs. (40), a similar but smoother trend is displayed and reaches the random state value when $\kappa_0 = 3\pi/2$.

The complementary state $\otimes_{k=1}^{2j}|0\rangle$ has a nonzero average as κ_0 approaches 0, both for the three- and the four-qubit cases. We have already discussed the origin of this in some detail for the three-qubit case. For a very large number of qubits we expect that classically the tunneling effect vanishes. This is borne out in Fig. 16, although surprisingly even for very large number of qubits for a range of κ_0 values close to 0, the formation of nonclassical states resulting in large average single-qubit entanglement is seen. The subsequent increase of entanglement for larger values of κ_0 is due to the destabilization of the period-4 orbit at $\kappa_0 = \pi$. A more detailed analysis is called for, including the study of entanglement between large blocks of spins which will distinguish between the nonclassical states produced when the system is near-integrable and the random states produced at much larger values of the parameter when the classical phase space is mixed or chaotic. A recent analysis in Ref. [66] uses an upper bound of the entanglement entropy using the Fannes-Audenaert inequality to argue for connections between entanglement and chaos and why states localized on the stable period-4 orbits can have large entanglement in the deep quantum regime.

V. CONCLUSIONS

Quest for an exactly solvable model is hard and often a matter of serendipity. In our work, we give exact solution for three- and four-qubit instances of the kicked top and explicitly derive expressions for the time-evolved state, reduced-density matrix, entanglement entropy, and its long-time average values. Our work provides interesting connections between a quantum system with few degrees of freedom and its classical limit that is nonintegrable and can exhibit chaos for high κ_0 values. For example, we find that the exactly solvable

three- and four-qubit instances of the kicked top provide insights into how entropy and entanglement thermalize in closed quantum systems in the sense of long-time averages approaching ensemble averages, as the classical limit approaches global chaos, as predicted by random matrix theory. Since we derive exact analytical results valid for all values of κ_0 , this will be further useful to study transition to thermalization in closed quantum systems. Experiments have already probed the three-qubit case, and it is worth mentioning that, in the light of our work, it should now be viewed as a study of thermalization in an integrable system rather than thermalization induced due to lack of sufficient number of conserved quantities [15]. It will be interesting to see at what spin size does the exact solvability of these models become intractable and whether or not that has a physical interpretation.

Even more remarkable is the entanglement dynamics at small values of the chaoticity parameter. This cannot be directly attributed to nonintegrability. For example, even for small κ_0 , in the case of the three-qubit $|0, 0\rangle$ state, we find an increase of entanglement with time, which can be attributed to the generation of highly nonclassical GHZ type states. We accurately predict timescales for such entanglement dynamics and found an excellent agreement with the numerics. Likewise, the $|\pi/2, -\pi/2\rangle$ state in the four-qubit case displays, for the same rotation angle, tunneling, and creation of GHZ states and we have described this in detail as well. In the near-integrable regime we exactly calculate tunneling splitting and show this to be in agreement with the numerics. To the best of our knowledge, ours is the first work to find a connection between tunneling splitting, the number of qubits and a system parameter. It is worth mentioning that entanglement generation occurs despite the initial state being localized on a stable island with phase space having almost no chaos. We believe our findings and analysis of entanglement generation at low values of κ_0 will contribute to the understanding of entanglement generation in dynamical systems and its connections to classical bifurcations, emergence of structures, and ergodicity in the phase space. This also complements our findings for higher values of κ_0 as well as the existing literature on the connections between entanglement generation and chaos.

Last, larger number of qubits can show genuine signatures of nonintegrability and chaos, and tunneling leads to creation of macroscopic superpositions that are generalized GHZ states. We hope our work raises new questions and adds to the discussion on the connections among integrability, quantum chaos, and thermalization. Since the multiqubit kicked top can be viewed as an analog quantum simulator, robustness of such a system to errors [67,68], especially in the regime where we generate highly nonclassical GHZ-like states and explore truly quantum phenomena like tunneling, will be of interest to the quantum information community. As an aside, we are able to give an alternate proof of the Pell identity satisfied by the Chebyshev polynomials.

ACKNOWLEDGMENT

We are grateful to the authors of Ref. [15] for generously sharing their experimental data, in particular to Pedram Roushan and Charles Neill for useful correspondence regarding the same.

APPENDIX: LINEAR ENTROPY OF AN ARBITRARY THREE-QUBIT PERMUTATION SYMMETRIC STATE

Considering a three-qubit state

$$|\psi_0\rangle = a_1|\phi_1^+\rangle + a_2|\phi_2^+\rangle + b_1|\phi_1^-\rangle + b_2|\phi_2^-\rangle, \quad (\text{A1})$$

each of the three qubits are initialized in the same state ($|\psi\rangle = \cos\frac{\theta_0}{2}|0\rangle + e^{-i\phi_0}\sin\frac{\theta_0}{2}|1\rangle$, in the computational bases), such that the initial state of the three-qubit system is $|\psi_0\rangle = \otimes^3|\psi\rangle$, where $\theta_0 \in [0, \pi]$ and $\phi_0 \in [-\pi, \pi]$. Repeated implementations of the unitary operator \mathcal{U} leads to $|\psi_n\rangle = \mathcal{U}^n|\psi_0\rangle$. We obtain single-party reduced-density operator by tracing out any of the two qubits of the three-qubit density operator ($\rho_n = |\psi_n\rangle\langle\psi_n|$), leading to

$$\rho_i = \begin{pmatrix} r & s \\ s^* & 1-r \end{pmatrix}, \quad (\text{A2})$$

where the elements of the density operator are given by

$$\begin{aligned} r &= \frac{1}{2} + \text{Re}\left(a_{1n}b_{1n}^* + \frac{1}{3}a_{2n}b_{2n}^*\right) \quad \text{and} \\ s &= \frac{1}{\sqrt{3}}\text{Re}(a_{1n}b_{2n}^* + b_{1n}a_{2n}^*) + \frac{i}{\sqrt{3}}\text{Im}(a_{1n}a_{2n}^* + b_{1n}b_{2n}^*) \\ &\quad - \frac{i}{3}(a_{2n} + b_{2n})(a_{2n}^* - b_{2n}^*). \end{aligned} \quad (\text{A3})$$

Where the coefficients $a_{1n} = a_1\alpha_n - a_2\beta_n^*$, $a_{2n} = a_1\beta_n + a_2\alpha_n^*$, $b_{1n} = i^n(b_1\alpha_n + b_2\beta_n^*)$, and $b_{2n} = i^n(b_2\alpha_n^* - b_1\beta_n)$. Linear entropy of the single qubit [Eq. (A2)] is thus given by

$$S_{(\theta_0, \phi_0)}^{(3)}(n, \kappa) = 2[r(1-r) - |s|^2]. \quad (\text{A4})$$

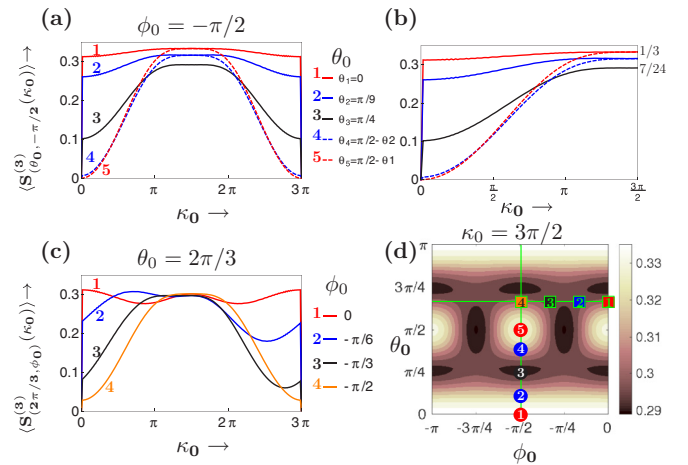


FIG. 17. [(a) and (b)] Time-averaged linear entropy [$\langle S_{(\theta_0, -\pi/2)}^{(3)} \rangle$] of a single-party reduced state vs. chaoticity parameter κ_0 . Different curves correspond to different initial states $|\theta_0, -\pi/2\rangle$ as labeled 1 to 5, along with explicit values of θ_0 given in the plot legends. These corresponding initial states $|\theta_0, \phi_0\rangle$ are also marked as numbered circles in the contour plot given in part (d). Part (c) contains the plots for $\langle S_{(2\pi/3, \phi_0)}^{(3)} \rangle$ vs. chaoticity parameter κ_0 for a fixed value of $\theta_0 = 2\pi/3$. Different curves correspond to different initial states, labeled by numbers 1 to 4, along with explicit values of ϕ_0 given in the plot legends. Respective initial states $|\theta_0, \phi_0\rangle$ are also marked as numbered squares (with a green border) in the contour plot given in part (d). Contour plot shown in part (d) corresponds to $\kappa_0 = 3\pi/2$.

Thus linear entropy is obtained as a function of the initial-state parameters (θ_0, ϕ_0) . Long-time average linear entropy is calculated numerically with $n = 1000$ for various initial states as shown in Fig. 17. Figures 17(a) and 17(c) show the variation of time-averaged entropy with chaoticity parameter for a period $2\pi j$. Pairs of complimentary θ_0 s saturate to the same values in the region around $\kappa_0 = 3\pi/2$. Figure 17(b)

highlights the range of values of average linear entropy at $\kappa_0 = 3\pi/2$, and a scale of similar range in Fig. 17(d) depicts that the linear entropy of a single-qubit reduced state for an arbitrary value of parameters (θ_0, ϕ_0) fall into this range. Further, we have obtained an explicit closed form expression for long-time average linear entropy for an arbitrary (θ_0, ϕ_0) at $\kappa_0 = 3\pi/2$, which is discussed in the main text.

-
- [1] P. Billingsley, Prime numbers and brownian motion, *Am. Math. Month.* **80**, 1099 (1973).
- [2] F. Haake, *Quantum Signatures of Chaos* (Spring-Verlag, Berlin, 1991).
- [3] A. Peres, *Quantum Theory: Concepts and Methods* (Kluwer Academic, New York, 2002).
- [4] M. Kuś, R. Scharf, and F. Haake, Symmetry versus degree of level repulsion for kicked quantum systems, *Z. Phys. B* **66**, 129 (1987).
- [5] M. Kus, J. Mostowski, and F. Haake, Universality of eigenvector statistics of kicked tops of different symmetries, *J. Phys. A: Math. Gen.* **21**, L1073 (1988).
- [6] K. Życzkowski, Indicators of quantum chaos based on eigenvector statistics, *J. Phys. A: Math. Gen.* **23**, 4427 (1990).
- [7] P. Gerwinski, F. Haake, H. Wiedemann, M. Kuś, and K. Życzkowski, Semiclassical Spectra without Periodic Orbits for a Kicked Top, *Phys. Rev. Lett.* **74**, 1562 (1995).
- [8] X. Wang, S. Ghose, B. C. Sanders, and B. Hu, Entanglement as a signature of quantum chaos, *Phys. Rev. E* **70**, 016217 (2004).
- [9] M. Lombardi and A. Matzkin, Entanglement and chaos in the kicked top, *Phys. Rev. E* **83**, 016207 (2011).
- [10] S. Ghose and B. C. Sanders, Entanglement dynamics in chaotic systems, *Phys. Rev. A* **70**, 062315 (2004).
- [11] V. Madhok, C. A. Riofrío, S. Ghose, and I. H. Deutsch, Information Gain in Tomography Quantum Signature of Chaos, *Phys. Rev. Lett.* **112**, 014102 (2014).
- [12] A. Piga, M. Lewenstein, and J. Q. Quach, Quantum chaos and entanglement in ergodic and nonergodic systems, *Phys. Rev. E* **99**, 032213 (2019).
- [13] U. T. Bhosale and M. S. Santhanam, Signatures of bifurcation on quantum correlations: Case of the quantum kicked top, *Phys. Rev. E* **95**, 012216 (2017).
- [14] S. Chaudhury, A. Smith, B. E. Anderson, S. Ghose, and P. S. Jessen, Quantum signatures of chaos in a kicked top, *Nature* **461**, 768 (2009).
- [15] C. Neill, P. Roushan, M. Fang, Y. Chen, M. Kolodrubetz, Z. Chen, A. Megrant, R. Barends, B. Campbell, B. Chiaro, A. Dunsworth, E. Jeffrey, J. Kelly, J. Mutus, P. J. J. O'Malley, C. Quintana, D. Sank, A. Vainsencher, J. Wenner, T. C. White, A. Polkovnikov, and J. M. Martinis, Ergodic dynamics and thermalization in an isolated quantum system, *Nat. Phys.* **12**, 1037 (2016).
- [16] A. C. Cassidy, D. Mason, V. Dunjko, and M. Olshanii, Threshold for Chaos and Thermalization in the One-Dimensional Mean-Field Bose-Hubbard Model, *Phys. Rev. Lett.* **102**, 025302 (2009).
- [17] L. F. Santos and M. Rigol, Onset of quantum chaos in one-dimensional bosonic and fermionic systems and its relation to thermalization, *Phys. Rev. E* **81**, 036206 (2010).
- [18] L. D'Alessio, Y. Kafri, A. Polkovnikov, and M. Rigol, From quantum chaos and eigenstate thermalization to statistical mechanics and thermodynamics, *Adv. Phys.* **65**, 239 (2016).
- [19] R. V. Jensen and R. Shankar, Statistical Behavior in Deterministic Quantum Systems with Few Degrees of Freedom, *Phys. Rev. Lett.* **54**, 1879 (1985).
- [20] J. M. Deutsch, Quantum statistical mechanics in a closed system, *Phys. Rev. A* **43**, 2046 (1991).
- [21] M. Srednicki, Chaos and quantum thermalization, *Phys. Rev. E* **50**, 888 (1994).
- [22] M. Rigol, D. Vanja, and O. Maxim, Thermalization and its mechanism for generic isolated quantum systems, *Nature* **452**, 854 (2009).
- [23] M. C. Bañuls, J. I. Cirac, and M. B. Hastings, Strong and Weak Thermalization of Infinite Nonintegrable Quantum Systems, *Phys. Rev. Lett.* **106**, 050405 (2011).
- [24] J. M. Deutsch, H. Li, and A. Sharma, Microscopic origin of thermodynamic entropy in isolated systems, *Phys. Rev. E* **87**, 042135 (2013).
- [25] T. Langen, R. Geiger, M. Kuhnert, B. Rauer, and J. Schmiedmayer, Local emergence of thermal correlations in an isolated quantum many-body system, *Nat. Phys.* **9**, 640 (2013).
- [26] L. D'Alessio and M. Rigol, Long-Time Behavior of Isolated Periodically Driven Interacting Lattice Systems, *Phys. Rev. X* **4**, 041048 (2014).
- [27] A. Lazarides, A. Das, and R. Moessner, Periodic Thermodynamics of Isolated Quantum Systems, *Phys. Rev. Lett.* **112**, 150401 (2014).
- [28] A. Lazarides, A. Das, and R. Moessner, Equilibrium states of generic quantum systems subject to periodic driving, *Phys. Rev. E* **90**, 012110 (2014).
- [29] A. Haldar, R. Moessner, and A. Das, Onset of floquet thermalization, *Phys. Rev. B* **97**, 245122 (2018).
- [30] A. M. Kaufman, M. Eric Tai, A. Lukin, M. Rispoli, R. Schittko, P. M. Preiss, and M. Greiner, Quantum thermalization through entanglement in an isolated many-body system, *Science* **353**, 794 (2016).
- [31] G. Clos, D. Porras, U. Warring, and T. Schaetz, Time-Resolved Observation of Thermalization in an Isolated Quantum System, *Phys. Rev. Lett.* **117**, 170401 (2016).
- [32] K. R. A. Hazzard, M. van den Worm, M. Foss-Feig, S. R. Manmana, E. G. Dalla Torre, T. Pfau, M. Kastner, and A. M. Rey, Quantum correlations and entanglement in far-from-equilibrium spin systems, *Phys. Rev. A* **90**, 063622 (2014).
- [33] M. C. Gutzwiller, *Chaos in Classical and Quantum Mechanics* (Springer-Verlag, New York, 1990).
- [34] V. Madhok, S. Dogra, and A. Lakshminarayan, Quantum correlations as probes of chaos and ergodicity, *Opt. Commun.* **420**, 189 (2018).

- [35] E. A. Yuzbashyan and B. S. Shastry, Quantum integrability in systems with finite number of levels, *J. Stat. Phys.* **150**, 704 (2013).
- [36] P. A. Miller and S. Sarkar, Signatures of chaos in the entanglement of two coupled quantum kicked tops, *Phys. Rev. E* **60**, 1542 (1999).
- [37] C. M. Trail, V. Madhok, and I. H. Deutsch, Entanglement and the generation of random states in the quantum chaotic dynamics of kicked coupled tops, *Phys. Rev. E* **78**, 046211 (2008).
- [38] A. Lakshminarayan, Entangling power of quantized chaotic systems, *Phys. Rev. E* **64**, 036207 (2001).
- [39] J. N. Bandyopadhyay and A. Lakshminarayan, Testing Statistical Bounds on Entanglement using Quantum Chaos, *Phys. Rev. Lett.* **89**, 060402 (2002).
- [40] J. N. Bandyopadhyay and A. Lakshminarayan, Entanglement production in coupled chaotic systems: Case of the kicked tops, *Phys. Rev. E* **69**, 016201 (2004).
- [41] A. J. Scott and C. M. Caves, Entangling power of the quantum baker's map, *J. Phys. A: Math. Gen.* **36**, 9553 (2003).
- [42] A. Lakshminarayan, S. C. L. Srivastava, R. Ketzmerick, A. Bäcker, and S. Tomsovic, Entanglement and localization transitions in eigenstates of interacting chaotic systems, *Phys. Rev. E* **94**, 010205(R) (2016).
- [43] M. J. Davis and E. J. Heller, Quantum dynamical tunneling in bound states, *J. Chem. Phys.* **75**, 246 (1981).
- [44] W. A. Lin and L. E. Ballentine, Quantum Tunneling and Chaos in a Driven Anharmonic Oscillator, *Phys. Rev. Lett.* **65**, 2927 (1990).
- [45] A. Peres, Dynamical Quasidegeneracies and Quantum Tunneling, *Phys. Rev. Lett.* **67**, 158 (1991).
- [46] *Tunneling in Complex Systems*, edited by S. Tomsovic (World Scientific, Singapore, 1998).
- [47] *Dynamical Tunneling-Theory and Experiment*, edited by S. Keshavamurthy (CRC Press, Boca Raton, FL, 2011).
- [48] G. J. Milburn, Simulating nonlinear spin models in an ion trap, [arXiv:quant-ph/9908037](https://arxiv.org/abs/quant-ph/9908037) (1999).
- [49] J. B. Ruebeck, J. Lin, and A. K. Pattanayak, Entanglement and its relationship to classical dynamics, *Phys. Rev. E* **95**, 062222 (2017).
- [50] U. T. Bhosale and M. S. Santhanam, Periodicity of quantum correlations in the quantum kicked top, *Phys. Rev. E* **98**, 052228 (2018).
- [51] G. Stamatiou and D. P. K. Ghikas, Quantum entanglement dependence on bifurcations and scars in non-autonomous systems. The case of quantum kicked top, *Phys. Lett. A* **368**, 206 (2007).
- [52] T. Prosen, Exact time-correlation functions of quantum ising chain in a kicking transversal magnetic fieldspectral analysis of the adjoint propagator in heisenberg picture, *Prog. Theor. Phys. Suppl.* **139**, 191 (2000).
- [53] A. Lakshminarayan and V. Subrahmanyam, Multipartite entanglement in a one-dimensional time-dependent ising model, *Phys. Rev. A* **71**, 062334 (2005).
- [54] R. J. Glauber and F. Haake, Superradiant pulses and directed angular momentum states, *Phys. Rev. A* **13**, 357 (1976).
- [55] R. R. Puri, *Mathematical Methods of Quantum Optics* (Springer, Berlin, 2001).
- [56] J. C. Mason and D. C. Handscomb, *Chebyshev Polynomials* (Chapman & Hall/CRC, Boca Raton, FL, 2002).
- [57] W. K. Wootters, Entanglement of Formation of an Arbitrary State of Two Qubits, *Phys. Rev. Lett.* **80**, 2245 (1998).
- [58] T. Yu and J. H. Eberly, Evolution from entanglement to decoherence of bipartite mixed "x" states, *Quantum Inf. Comput.* **7**, 459 (2007).
- [59] S. K. Mishra, A. Lakshminarayan, and V. Subrahmanyam, Protocol using kicked ising dynamics for generating states with maximal multipartite entanglement, *Phys. Rev. A* **91**, 022318 (2015).
- [60] A. Seshadri, V. Madhok, and A. Lakshminarayan, Tripartite mutual information, entanglement, and scrambling in permutation symmetric systems with an application to quantum chaos, *Phys. Rev. E* **98**, 052205 (2018).
- [61] D. F. V. James, P. G. Kwiat, W. J. Munro, and A. G. White, Measurement of qubits, *Phys. Rev. A* **64**, 052312 (2001).
- [62] M. Steffen, M. Ansmann, R. C. Bialczak, N. Katz, E. Lucero, R. McDermott, M. Neeley, E. M. Weig, A. N. Cleland, and J. M. Martinis, Measurement of the entanglement of two superconducting qubits via state tomography, *Science* **313**, 1423 (2006).
- [63] E. Lucero, M. Hofheinz, M. Ansmann, R. C. Bialczak, N. Katz, M. Neeley, A. D. O'Connell, H. Wang, A. N. Cleland, and J. M. Martinis, High-Fidelity Gates in a Single Josephson Qubit, *Phys. Rev. Lett.* **100**, 247001 (2008).
- [64] D. M. Greenberger, M. A. Horne, and A. Zeilinger, in *Going Beyond Bell's Theorem* (Springer Netherlands, Dordrecht, 1989), pp. 69–72.
- [65] D. M. Greenberger, M. A. Horne, A. Shimony, and A. Zeilinger, Bell's theorem without inequalities, *Am. J. Phys.* **58**, 1131 (1990).
- [66] M. Kumari and S. Ghose, Untangling entanglement and chaos, *Phys. Rev. A* **99**, 042311 (2019).
- [67] P. Hauke, F. M. Cucchietti, L. Tagliacozzo, I. Deutsch, and M. Lewenstein, Can one trust quantum simulators? *Rep. Prog. Phys.* **75**, 082401 (2012).
- [68] D. L. Shepelyansky, Quantum chaos and quantum computers, *Phys. Scr.* **T90**, 112 (2001).